Diphenyltin^{IV}dithiocarbamate Macrocyclic Complexes Derived from 4,4'-Bis(2-(alkylamino)acetamido)diphenyl ether, CS_2 and Ph_2SnCl_2: Synthesis, Characterization, DFT study and *in vitro* Apoptosis Inducing-Cytotoxic Activity

Abstract

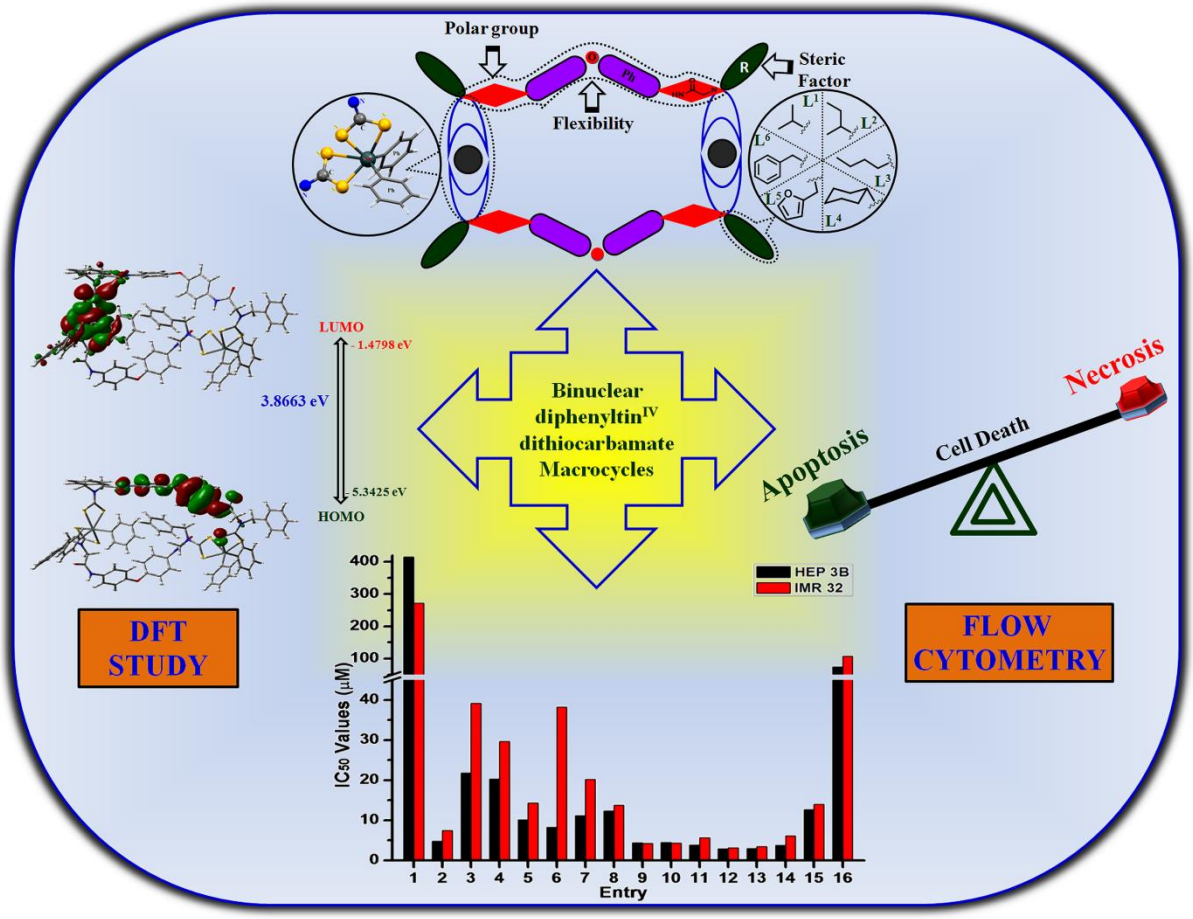

Six binuclear diphenyltin^{IV}dithiocabamate macrocyclic complexes were efficiently synthesized through self-assembly process of diamino precursors, CS_2 and Ph_2SnCl_2. The geometry of all the compounds has been optimized by DFT method. The MTT assay clearly revealed extremely higher *in-vitro* cytotoxicity activity of binuclear Ph_2Sn^{IV}dithiocarbamate macrocyclic complexes 1-6 against HEP 3B and IMR 32; also they exhibit better potency than cisplatin, a well known antineoplastic drug. These scaffolds, with excellent IC_{50} values were explored as a novel class of active chemical agents to induce apoptosis, required for major therapeutic implication in cancer therapy.

4.1. Introduction

The pharmaceutical development is one of the prime concerns of current research in the battle against cancer wherein large-scale synthesis for lower cost of production of generic and proprietary products is a big challenge. The efforts in the evaluation of anticancer drugs have been shifted to non-platinum metal-based agents[1] who do not only depend on direct DNA damage for their activity but they may also engage proteins and enzymes to avoid significant side effects and the emergence of drug resistance associated with platinum chemotherapeutics.[2] Since the initial discovery in 1972 on retardation of tumor growth in mice by triphenyltin acetate[3] a number of reports highlight the organotin compounds as potential biologically active metallopharmaceuticals[2, 4] with promising in vitro and in vivo antitumor activity over a range of tumor cell lines. Although, the organotin moiety is crucial for cytotoxicity an elegant choice of the ligand fragment can efficiently modulate the cytotoxic activity of the organotin^{IV} complexes as well as it can minimize the drawbacks. Studies have already underlined the relevance to organotin^{IV} complexes with sulfur donor ligands due to their unique stereo-electronic properties. In fact, the sulfur atoms in molecules and donor ligand plays a vital role in transporting and addressing the molecule to the targets as well as in the protection of pharmacophore against untimely exchanges with biomolecules.[5] These molecules in particular are currently under study as chemoprotectants in platinum-based chemotherapy because these are shown to exhibit high anticancer activity along with reduced toxicity, compared to cisplatin and analogous compounds.[6] Further investigations reveal 2-3 fold more cytotoxicity of these complexes under slightly acidic conditions (pH 6.8) as compared to pH 7.4.[7] This effect is remarkable, as in solid tumors slightly acidic conditions were frequently observed due to anaerobic fermentation of glucose secreting lactic acid in tumor tissue.[8] Apart from this, the strong binding ability and diverse binding modes towards various transiton/ non-transition metal ions in different oxidation states make[4e, 9-12] the sulfur donor ligands especially dithiocarbamates highly promising towards the development of coordination-driven self-assembled diverse structures including macrocycles exhibiting potential applicability in drug delivery, two-phase transport, biosensing.[13, 14-16] and found very effective in tumor treatment in vitro and in vivo for broad spectrum of cancer cells.[17]

In recent past, multinuclear platinum-based, third-generation drugs bearing variable length biogenic polyamines as bridging linkers has been emerged as a new class of compounds with great clinical importance.[18] They were found to be distinct from their mononuclear counterparts in terms of DNA binding features, yielding adducts containing "long-distance" intra- and interstrand cross-links.[18g,19] Moreover, these polynuclear metal complexes have often been reported to overcome acquired cisplatin resistance [20] probably because of a distinct mechanism of DNA interaction that results in different types of drug-induced DNA lesions. Although binuclear macrocyclic dithiocarbamate complexes have been widely explored in supramolecular chemistry[21] and excellent biological properties exhibited by mononuclear organotin^{IV}dithiocarbamate complexes,[4] surprisingly no reports are available on biological investigation of binuclear organotin^{IV}dithiocarbamate macrocyclic complexes in spite of their capabilities to provide mutual effects associated with functionalized macrocycles and organotin centres towards high degree of potency as well as selectivity. It is established that a simple chemical modification in the structure of a certain compound may alter its DNA binding properties and/or the relative amounts of interstrand crosslinks in double-stranded DNA, thus governing its antiproliferative and cytotoxic activity.

Despite of the unique characteristics of macrocyclic scaffolds and sulphur donor ligands in biological processes (*vide supra*), the polymetallic dithiocarbamates macrocyclic complexes are surprisingly unexplored in medicinal chemistry, though these have been exhaustively studied in supramolecular chemistry, especially host-guest reactivity study.[9]

These observations motivated us for the development of organotin based macrocycles which would exhibit high degree of potency and selectivity in medicinal chemistry. In this contribution, we report a facile synthesis, characterization, computational studies and in vitro cytotoxic activity against human cancer cell lines HEP 3B (Hepatoma) and IMR 32 (Neuroblastoma) of 4,4'-bis(2-chloroacetamido)diphenyl ether[22] (**L'**), 4,4'-bis(2-(alkylamino)acetamido)diphenyl ethers (**L^1-L^6**) and series of binuclear organotin^{IV}dithiocarbamate macrocyclic complexes [$(Ph_2Sn^{IV})_2$-μ^2-bis-{(κ^2*S,S*-$S_2CN(R)CH_2CONHC_6H_4)_2O$}] {R = ^{i}*Pr* (**1**), ^{s}*Bu* (**2**), ^{n}*Bu* (**3**), *Cy* (**4**), 2-*furfuryl* (**5**) or *benzyl* (**6**)}. The presence of more than one metal

center in these multifunctional complexes **1-6** may confer higher efficacy and specificity towards DNA binding.

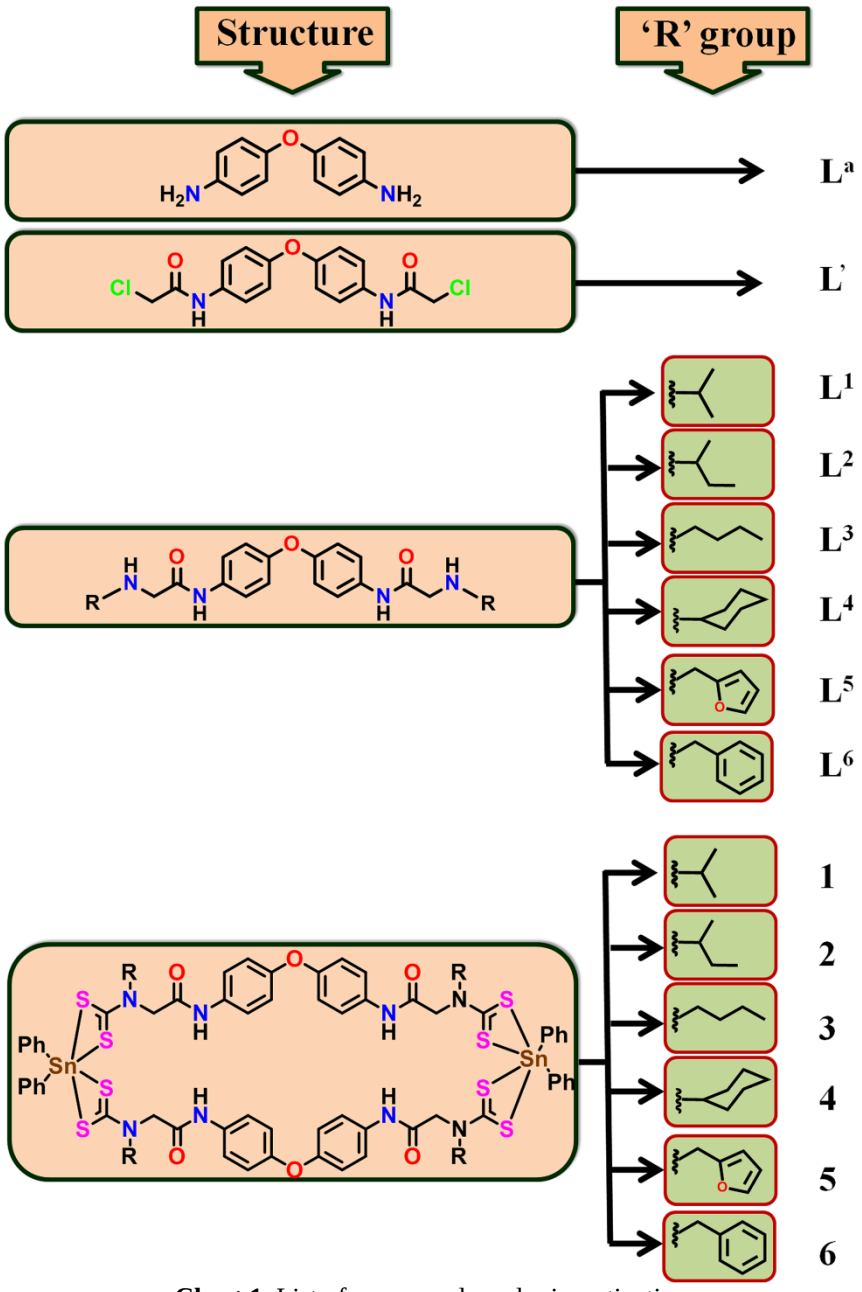

Chart 1. List of compounds under investigation.

4.2. Experimental Section

4.2.1. Synthesis of 4,4'-bis(2-chloroacetamido)diphenyl ether (L')

To a solution of 1 equivalent (10 mmol; 2 g) of 4,4'-diaminodiphenyl ether in 50 mL dichloromethane containing 3 equivalent (30 mmol; 3.036 g) of freshly distilled triethyl amine 3 equivalents (30 mmol; 3.388 g) of chloroacetyl chloride was added drop wise over a period of half an hour at 0 ºC. The reaction mixture was allowed to

stir for 2.5 hrs at room temperature and reaction progress was monitored by TLCs. Product was extracted using 100 mL dichloromethane thereafter dichloromethane extracts were washed with 2 × 100 mL saturated Na_2CO_3 solution followed by distilled water. Dichloromethane layer was dried using anhydrous Na_2SO_4 and solvent was evaporated under vacuum to recover white solid. The product was dried under vacuum; sample was taken for analysis and used for the synthesis of diamine precursors **L^1-L^6**. The reaction scheme is outlined below,

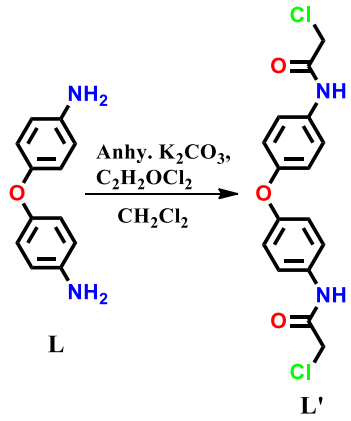

Scheme 1. Reaction scheme for 4,4'-bis(2-chloroacetamido)diphenyl ether (**L'**).

4.2.2. General synthetic procedure for of secondary diamine precursors (L^1-L^6)

To a solution of corresponding amines *i.e.* isopropyl amine (591 mg, 10 mmol), 2-butyl amine (731 mg 10 mmol), 1-butyl amine (731 mg 10 mmol), cyclohexyl amine (595 mg, 6 mmol), 2-furfuryl amine (583 mg, 6 mmol) or benzyl amine (643 mg, 6 mmol) in 50 mL of absolute ethanol was added 3 equivalent of anhydrous K_2CO_3 (6 mmol; 829 mg) and reaction mixture was allowed to warm slightly for 5 minutes. To this mixture, 4,4'-bis(2-chloroacetamido)diphenyl ether (706 mg, 2 mmol) was added and the reaction mixture was refluxed for 5-6 hrs. The progress of the reaction was monitored by TLC. The reaction mixture was allowed to cool at room temperature and the solvent was evaporated under vacuum. The solid residue was washed with 2 × 25 mL distilled water, followed by n-hexane and diethyl ether to yield new diamines **L^1-L^6** in good yields. These derivatives were further purified by column chromatography using neutral alumina and ethyl acetate/ n-hexane solvent mixture as an eluent. These were stored under a nitrogen atmosphere and samples were taken for analysis. This reaction is outlined in scheme 2.

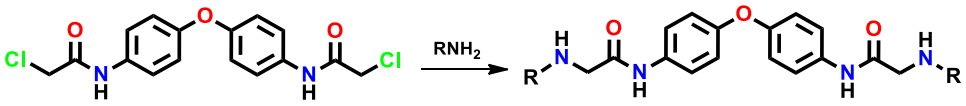

R = ^{i}Pr (**L^{1}**); ^{s}Bu (**L^{2}**); ^{n}Bu (**L^{3}**); Cy (**L^{4}**); 2-furfyryl (**L^{5}**); Bn (**L^{6}**).

Scheme 2. Reaction scheme for synthesis of diamine precursors **L^{1}-L^{6}**.

4.2.3. Synthesis of binuclear diphenyltin^{IV}dithiocarbamate macrocyclic complexes 1-6

In a typical procedure, 4,4'-bis(2-(isopropylamino)acetamido)diphenyl ether (199 mg 0.5 mmol), 4,4'-bis(2-(sec-butylamino)acetamido)diphenyl ether (213 mg, 0.5 mmol), 4,4'-bis(2-(n-butylamino)acetamido)diphenyl ether (213 mg, 0.5 mmol), 4,4'-bis(2-(cyclohexylamino)acetamido)diphenyl ether (239 mg, 0.5 mmol), 4,4'-bis(2-(2-furfurylamino)acetamido)diphenyl ether (237 mg, 0.5 mmol) or 4,4'-bis(2-(benzylamino)acetamido)diphenyl ether (247 mg, 0.5 mmol) and excess amount of CS_2 *ca* (0.5 mL, 8.32 mmol) were added in 20 mL of Et_3N solvent. The reaction mixture was allowed to stir for 12 hr at room temperature wherein a change in colour from colourless to pale yellow was observed. To this mixture, diphenyltin dichloride (189 mg, 0.55 mmol) was added with rigorous stirring and the reaction was allowed to continue for 8 h at room temperature. The residue was filtered in a glass sintered crucible and washed several times with distilled triethyl amine followed by n-hexane and diethyl ether. The white residue (in case of **1-4**) and pale yellow residue (in case of **5-6**) were dried under vacuum and stored under nitrogen atmosphere before samples were taken for analysis. This synthetic methodology is outlined in scheme 3.

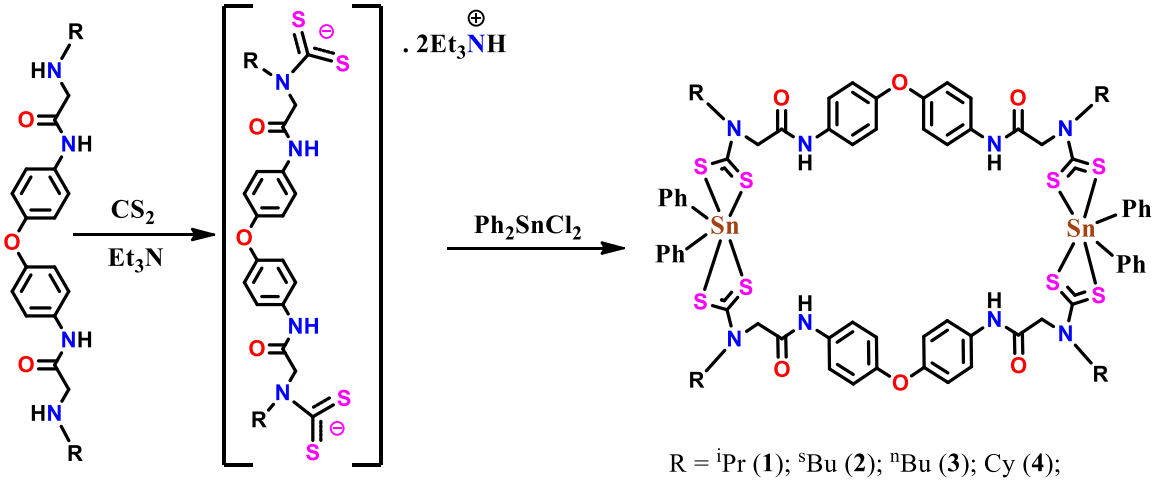

L^{1}-L^{6} **Prepared *in situ***

R = ^{i}Pr (**1**); ^{s}Bu (**2**); ^{n}Bu (**3**); Cy (**4**); 2-furfyryl (**5**); Bn (**6**).

Scheme 3. One pot synthetic protocol for a series of binuclear Ph_2Sn^{IV}dithiocarbamate macrocyclic complexes **1-6**.

Table 1. Micro-, mass- and IR analysis data for compounds **L^1-L^6** and **1-6**.

Entry	Molecular Formula (MW)	Yield (%)	Mp (˚C)	Elemental Analysis (%) Found (calculated)				ES-MS (m/z)	IR data (KBr disk) υ_{max}/cm^{-1}
				C	H	N	S		
L'	$C_{16}H_{14}Cl_2N_2O_3$ (353.20)	99	232	...	...	...	...	375.04, 377.04 (M+Na)	...
L^1	$C_{22}H_{30}N_4O_3$ (398.50)	85	120 °C dec	66.25 (66.31)	7.65 (7.59)	14.01 (14.06)	...	398.41 (M+H)	3490w, 3142w 2965m, 2622m, 2297w, 1871w, 1692s, 1679s, 1629s, 1501m, 1408s, 1368m, 1226m, 1073m, 1008s, 978s, 831s, 703s, 663s.
L^2	$C_{24}H_{34}N_4O_3$ (426.55)	82	150 °C dec	67.47 (67.58)	8.15 (8.03)	13.21 (13.13)	...	427.44 (M+H)	3459m, 2963m, 2626s, 2297w, 2102w, 1865w, 1691s, 1652s, 1635s, 1501m, 1403s, 1370s, 1227m, 1007s, 970s, 832s, 703s, 663s.
L^3	$C_{24}H_{34}N_4O_3$ (426.55)	90	200 °C dec.	67.57 (67.58)	8.43 (8.03)	13.07 (13.13)	...	427.55 (M+H)	3278s, 3053m, 2958s, 2931s, 2870m, 1888w, 1690s, 1677s, 1605s, 1510s, 1499s, 1409s, 1376m, 1305s, 1220s, 1166m, 1104m, 1013m, 948m, 878m, 832s, 706m, 513w.
L^4	$C_{28}H_{38}N_4O_3$ (478.63)	83	137.7	70.37 (70.26)	8.05 (8.00)	11.75 (11.71)	...	479.28 (M+H)	3335s, 3262s, 3031w, 2926s, 2852s, 1689s, 1670s, 1593s, 1522s, 1499s, 1449m, 1407s, 1374m, 1327w, 1304s, 1242s, 1219s, 1194m, 1132s, 1109s, 1012w, 930w, 877m, 844s, 821s, 768w, 721w, 515s, 492m.
L^5	$C_{26}H_{26}N_4O_5$ (474.51)	89	250 °C dec.	65.87 (65.81)	5.65 (5.52)	11.83 (11.81)	...	--	3319s, 2850m, 2810m, 1690s, 1657s, 1601w, 1560m, 1500s, 1409s, 1335m, 1303w, 1224s, 1165w, 1147m, 1107w, 1011s, 878m, 832s, 740w, 703w, 662w, 599w, 521s.
L^6	$C_{30}H_{30}N_4O_3$ (494.58)	93	128.4	72.88 (72.85)	6.15 (6.11)	11.31 (11.33)	...	495.26 (M+H), 517.23, 518.24 (M+Na)	3327m, 3268s, 3028w, 2885w, 2828w, 2806w, 1688s, 1670s, 1592m, 1544s, 1522s, 1498s, 1450w, 1406s, 1365w, 1329w, 1304w, 1244s, 1218s, 1195m, 1130m, 1107m, 1029w, 981w, 931w, 878w, 855w, 839w, 815s, 774w, 741s, 697m, 517s, 494w, 481w, 470w.
1	$C_{72}H_{76}N_8O_6S_8Sn_2$ (1643.36)	89	>90 °C dec.	52.54 (52.62)	4.59 (4.66)	6.89 (6.82)	15.70 (15.61)	...	3318w, 3065s, 3047s, 2991m, 2599w, 2360w, 1660s, 1640s, 1605s, 1499s, 1481w, 1429s, 1407m, 1371w, 1300w, 1224s, 1078s, 1008m, 998w, 832s, 722s, 694s, 660w, 619w, 570s, 473m, 431s.

2	$C_{76}H_{84}N_8O_6S_8Sn_2$ (1699.47)	85	>80 °C dec.	53.63 (53.71)	5.07 (4.98)	6.52 (6.59)	15.01 (15.09)	...	3386w, 3065s, 3047s, 2973m, 2599w, 2356w, 1660s, 1651s, 1610s, 1500s, 1481m, 1429s, 1408s, 1373m, 1300w, 1228s, 1156w, 1108m, 1078s, 1008s, 998s, 875w, 833s, 723s, 694s, 661m, 619w, 570s, 473s, 430s.
3	$C_{76}H_{84}N_8O_6S_8Sn_2$ (1699.47)	91	>110 °C dec.	53.73 (53.71)	5.09 (4.98)	6.65 (6.59)	15.05 (15.09)	...	3354m, 3065w, 3047w, 2978s, 2943s, 2882s, 2739s, 2604s, 2531s, 2497s, 2359s, 2139w, 1684s, 1675s, 1479s, 1444s, 1429s, 1398s, 1384s, 1365m, 1331w, 1293w, 1260w, 1229w, 1172s, 1078s, 1037s, 998w, 851m, 807m, 722s, 694s, 660w, 619w, 570s, 472s, 430s.
4	$C_{84}H_{92}N_8O_6S_8Sn_2$ (1803.62)	93	>130 °C dec.	55.86 (55.94)	5.10 (5.14)	6.17 (6.21)	14.30 (14.22)	...	3438m, 3255w, 3196w, 3133w, 3049w, 2978m, 2937s, 2856m, 2738w, 2677m, 2615m, 2604m, 2496m, 1688s, 1613m, 1558s, 1499s, 1478s, 1452s, 1409m, 1305m, 1225s, 1169m, 1107m, 1073w, 1036m, 1012m, 998w, 969w, 896w, 876m, 834s, 731m, 694s, 620w, 570m, 514m, 471w, 446w.
5	$C_{80}H_{68}N_8O_{10}S_8Sn_2$ (1795.38)	81	>100 °C dec.	53.47 (53.52)	3.92 (3.82)	6.23 (6.24)	14.35 (14.29)	...	3298m, 3064m, 3046m, 2978s, 2943s, 2739m, 2604s, 2531m, 2497s, 2359m, 1885w, 1670s, 1611s, 1505s, 1446m, 1428m, 1398m, 1330w, 1304m, 1221s, 1170s, 1106s, 1076s, 1036s, 1012m, 942w, 875m, 835s, 722s, 694s, 660w, 569s, 520w, 473m, 438s.
6	$C_{88}H_{76}N_8O_6S_8Sn_2$ (1835.54)	97	>130 °C dec.	57.69 (57.58)	4.29 (4.17)	6.11 (6.10)	14.05 (13.98)	...	3282m, 3064s, 3046s, 2992m, 2352w, 1958w, 1887w, 1688s, 1680s, 1674s, 1606s, 1497s, 1453s, 1429s, 1409s, 1304m, 1220s, 1161s, 1106m, 1079s, 1013w, 997s, 946w, 876w, 833s, 721s, 694s, 619w, 570s, 512w, 472m, 433s.

Table 2. NMR spectral data for **L^1-L^6** and **1-6**.

Entry	NMR Data (ppm)			^{119}Sn (DMSO-d6)
	^{1}H and ^{13}C			
	^{1}H NMR	^{13}C NMR	DEPT-135	
L'	10.334(s, 2H, NH); 7.580(d, 4H, Ph); 7.985(dd, 4H, Ph); 4.242(s, 4H, CH_2).	164.90 (CO); 153.34, 134.47, 121.60, 119.29; (all corresponds to the carbons of Ph), 43.96 (CH_2).	121.59, 119.30 (all CH of Ph); 43.96 (CH_2)	...
L^1	9.499 (s, 2H, CON*H*), 7.579 (m, 4H, *Ph*), 7.010 (m, 4H, *Ph*), 3.390 (d, 4H, NCH_2CO), 2.885 (m, 2H, C*H* of ^{i}*Pr*), 1.45 (bs, 2H, N*H*), 1.122 (m, 12H, CH_3 of ^{i}*Pr*)	170.58 (*C*O), 152.28, 133.98, 121.09, 121.01, 118.52; (all corresponds to the carbons of *Ph*), 50.82 (N*C*H_2CO), 49.93, 49.91(*C*H of ^{i}*Pr*), 23.12(*C*H_3 of ^{i}*Pr*).	121.09, 121.01, 118.51 (*C*H of *Ph*), 50.82 (N*C*H_2CO), 49.94 (*C*H of ^{i}*Pr*), 23.12, 23.03 (*C*H_3 of ^{i}*Pr*).	...
L^2	9.550 (s, 2H, CON*H*), 7.510 (m, 4H, *Ph*), 7.050 (m, 4H, *Ph*), 3.398 (s, 4H, NCH_2CO), 2.65 (m, 2H, NC*H* of ^{s}*Bu*), 1.323 (m, 4H, CH_2 of ^{s}*Bu*), 1.105 (d, 6H, CH_3 of ^{s}*Bu*), 0.987 (m, 6H, CH_3 of ^{s}*Bu*).	170.53(*C*O), 153.65, 133.14, 121.64, 121.57, 119.19, 119.03 (all corresponds to the carbons of *Ph*), 51.64 (*C*H of ^{s}*Bu*), 50.56 (N*C*H_2CO), 29.81, 29.72 (*C*H_2 of ^{s}*Bu*), 20.20, 20.10 (*C*H_3 of ^{s}*Bu*).	121.65, 121.57, 119.19, 119.03 (*C*H of *Ph*), 51.64 (*C*H of ^{s}*Bu*), 50.56 (N*C*H_2CO), 29.89 (*C*H_2 of ^{s}*Bu*), 20.21, 20.10 (*C*H_3 of ^{s}*Bu*).	...
L^3	9.408 (s, 2H, CON*H*), 7.565 (m, 4H, *Ph*), 6.959 (m, 4H, *Ph*), 3.398 (t, 4H, NCH_2CO), 2.696 (q, 4H, CH_2 of ^{n}*Bu*), 1.743 (broad s, 2H, N*H*), 1.325 (m, 8H, CH_2 of ^{n}*Bu*), 0.960 (m, 6H, CH_3 of ^{n}*Bu*).	170.296 (*C*O); 153.20, 153.03, 134.75, 134.53, 121.3, 119.16 (all corresponds to the carbons of *Ph*), 55.67 (N*C*H_2CO), 50.98, (N*C*H_2 of ^{n}*Bu*), 29.99, 29.51, 20.28, 20.05 (*C*H_2 of ^{n}*Bu*); 14.31, 14.17 (*C*H_3 of ^{n}*Bu*).	...	...
L^4	) 9.494 (s, 2H, CON*H*), 7.560 (d, 4H, *Ph*), 6.980 (d, 4H, *Ph*), 3.409 (s, 4H, NCH_2CO), 2.193 (bs, 2H, N*H*), 2.462 (t, 2H, NC*H* of *Cy*), 1.943-1.191(m, 20H, CH_2 of *Cy*).	170.44 (*C*O); 152.97, 134.68, 121.16, 119.13 (all corresponds to the carbons of *Ph*), 56.67 (N*C*H_2CO); 50.20 (*C*H of *Cy*); 32.93, 26.11, 24.80 (*C*H_2 of *Cy*).	...	...
L^5	9.312 (s, 2H, CON*H*), 7.60 (m, 4H, *Ph*), 7.050 (m, 4H, *Ph*), 6.340 (t, 2H, *furanyl*), 6.250 (d, 4H, *furanyl*), 3.698 (s, 4H, NCH_2CO), 3.434 (s, 4H, CH_2 of *furanyl*).	169.48, 163.95 (*C*O), 157.15, 157.00, 152.43, 142.46, 134.17, 133.97, 126.58, 121.63, 121.18, 120.34, 118.67, 118.57, 110.35, 107.94 (all corresponds to *Ph*/ *furanyl* carbons), 69.97, 67.33 (*C*H_2 of *furfuryl*, 53.60, 51.86 (N*C*H_2CO).	126.59, 121.63, 121.18, 120.34, 118.67, 118.57, 110.35, 107.94 (CH of *Ph*/ *furanyl*), 69.96, 67.34 (*C*H_2 of *furfuryl*) 53.59, 51.85 (N*C*H_2CO).	...
L^6	9.837 (s, 2H, CON*H*), 7.626-6.940 (m, 18H, Ph), 3.745 (s, 4H, NCH_2CO), 3.629 (s, 4H, NCH_2Ph), 2.8 (bs, 2H, NH).	170.36 (*C*O); 153.03, 140.74, 134.73, 128.66, 128.50, 127.19, 121.35, 119.13 (all corresponds to the carbons of *Ph*), 53.05 (N*C*H_2CO), 52.36 (N*C*H_2Ph).	129.16, 128.67, 128.51, 127.20, 121.33, 119.13 (*C*H of *Ph*), 53.02 (CH_2 of N*C*H_2CO), 52.33 (N*C*H_2Ph).	...
1	(DMSO-d6): 10.480-10.393 (CON*H*), 7.947-6.804 (C*H* of *Ph*), 4.669, 4.459 (NCH_2CO), 3.965 (C*H* of ^{i}*Pr*), 1.059 (CH_3 of ^{i}*Pr*).	(DMSO-d6): 136.31, 136.12, 135.94, 128.52, 128.33, 127.60, 124.70, 121.00, 120.82, 113.26, 112.89(all corresponds to the carbons of *Ph*); 62.06 (N*C*H_2CO); 52.43, 51.72 (*C*H of ^{i}*Pr*); 20.38(*C*H_3 of ^{i}*Pr*).	...	-238.595

2	(DMSO-d6): 10.683 (CON*H*), 7.667-6.775 (C*H* of *Ph*), 4.623, 4.458 (NCH_2CO), 3.935 (NC*H* of ^{s}*Bu*), 1.80 (CH_2 of ^{s}*Bu*), 1.022 (CH_3 of ^{s}*Bu*).	(DMSO-d6): 136.58, 136.31, 136.12, 135.99, 128.49, 128.06, 127.67, 127.57, 122.00, 121.86, 121.27, 120.85, 120.75(all corresponds to the carbons of *Ph*), 66.68 (N*C*H_2CO), 53.5-52.7 (*C*H of ^{s}*Bu*), 27.61(*C*H_2 of ^{s}*Bu*), 15.37, 15.16, 12.94, 11.49(*C*H_3 of ^{s}*Bu*).	...	-238.469
3	9.629, 9.557 (CON*H*), 8.077-6.880 (C*H* of *Ph*), 4.710 (NCH_2CO), 3.385-0.909 (CH_2, CH_3 of ^{n}*Bu*).	170.26 (*C*O); 153.05-119.19 (all corresponds to the carbons of *Ph*); 59.63, 58.51(N*C*H_2CO), 55.66, 55.40 (N*C*H_2 of ^{n}*Bu*), 29.52, 28.60, 20.29, 19.85 (*C*H_2 of ^{n}*Bu*), 14.34, 14.10 (*C*H_3 of ^{n}*Bu*).	...	-236.694
4	10.353 (CON*H*), 7.891-6.927 (C*H* of *Ph*), 4.612 (NCH_2CO), 3.420 (C*H* of *Cy*), 2.822-1.077(CH_2 of *Cy*).	171.44 (*C*O); 153.01-119.20 (all corresponds to the carbons of *Ph*); 56.64 (N*C*H_2CO); 52.83 (*C*H of *Cy*); 29.81, 29.61, 29.28, 26.01, 25.79, 25.53, 25.37, 24.98 (*C*H_2 of *Cy*).	...	-236.338
5	10.276-9.832(CON*H*), 7.805-6.376(C*H* of *Ph*/ *furfuryl*), 3.989 (br, NCH_2CO/ *furfuryl*).	164.50(*C*O), 156.34, 154.18, 151.87, 148.87, 147.55, 143.74, 142.51, 136.21, 135.32, 128.95, 128.44, 128.05, 127.56, 121.94, 121.31, 120.19, 118.26, 111.14, 110.73, 109.97, 107.48 (all corresponds to the carbons of *Ph*/ *furanyl*), 70.54, 66.61 (*furfuryl carbons*), 53.38, 52.11 (N*C*H_2CO).	...	-241.188
6	10.303, 9.949 (CON*H*), 7.994-6.933(C*H* of *Ph*), 3.758, 3.313 (NCH_2CO/ CH_2Ph).	170.104, 169.85 (CO); 152.97-119.11 (all corresponds to the carbons of Ph); 52.87, 52.17 (N*C*H_2CO/ *C*H_2Ph).	...	-236.265

4.2.4. In vitro cytotoxicity study

MTT assay for cell viability/ proliferation: The MTT assay was used to determine cell growth inhibition with some modifications.[22] 4,4'-bis(2-chloroacetamido)diphenyl ether (**L**), diamine precursors (**L^1-L^6**) and binuclear diphenyltin^{IV}dithiocarbamate complexes (**1-6**) were dissolved in DMSO and then diluted with water. The content of DMSO in each sample was 1%. Cells were seeded in 96-well plates at a density of 1×10^3 cells per well and then incubated for 24 h. Thereafter the cells were treated with different concentrations of compounds reported in this paper for 14 h. Under the similar experimental conditions cisplatin was also screened against both the cell lines. Finally the media were removed and the culture was incubated with 20 µL of media containing 5 mg/ml stock solution of MTT in PBS and 60 µL of DMEM for 6 h at 37 °C in 5% CO_2 incubator. The resultant formazan crystal formed by metabolically viable cells was dissolved by adding DMSO. The optical density was measured at 570 nm by ELISA reader (METERTECH-∑960). The number of viable cells was proportional to the extent of formazan production.

Annexin V/PI Double Staining for Cell Death Analysis: Cell death analysis was performed using annexin V alexa Fluro 4888 and propidium iodide apoptosis kit, procured from Himedia. For apoptosis examination, HEP 3B and IMR 32 cells (5×10^6 cells/mL) were treated with selective compounds ($^1/_3$ of the IC_{50} concentration) for 16 hours. After washing in PBS, 1×10^6 cells were resuspended in 100µl of annexin binding buffer. FITC-Annexin V and propidium iodide were added and then incubated for 15 minutes at room temperature in the dark. After the incubation period, 400 µL of annexin-binding buffer was added then kept in an ice bath for 5 minutes. Cells were centrifuged and fixed in 1% formalin. Cells were resuspended in 1% FBS and 0.5% in BSA after centrifugation. Then cells were analyzed by flow cytometry (BD FACSAria III).

4.3. Results and Discussion

4.3.1. Syntheses and Characterization

Our recent investigation[23] on the antitumor activity of diamino/ bisimine derivatives of 4,4'diaminodiphenyl ether against human cancer cell lines has inspired us to derivatize the lead compound "4,4'diaminodiphenyl ether" further in search of a potent antitumor agent. Thus a novel series of secondary diamino 4,4'-bis(2-

(alkylamino)acetamido)diphenyl ether (**L^{1}-L^{6}**) derivatives were synthesized in >80 % yields by the nucleophilic substitution of α-chloro substituents of 4,4'-bis(2-chloroacetamido)diphenyl ether (**L'**) with a number of primary amines. Further with the hope that complexation of these diamino precursors **L^{1}-L^{6}** with biologically active Ph_2Sn^{IV} fragment[4] would enhance the cytotoxicity (*vide supra*), a new series of binuclear Ph_2Sn^{IV}dithiocarbamate macrocyclic scaffold **1-6** bearing functionalized polar linkers have been designed and synthesized. The one-pot reaction protocol involving self-assembly of the corresponding diamine **L^{1}-L^{6}** with CS_2 and Ph_2SnCl_2 affords access to a series of binuclear Ph_2Sn^{IV}dithiocarbamate macrocyclic scaffolds **1-6** quantitatively. These complexes bearing several aromatic and amide functionalities in the linker framework and biologically active Ph_2Sn^{IV} would mutually facilitate the interaction with biomolecules through potential donor-acceptor interactions such as hydrogen bonding, CH-π, π-π interactions. All the newly synthesized compounds, viz **L'**, **L^{1}-L^{6}** and binuclear complexes **1-6** (chart 1) were characterized by microanalysis and relevant spectroscopic techniques. Although these compounds could not be obtained in the crystalline state, their composition and structures were elucidated by microanalysis and spectroscopic data.

The elemental analysis data are in good agreement with their compositions as per the proposed structures which are mutually supported by subsequent spectroscopic data and theoretical studies. The characteristic IR bands appeared in the range of 1499–1446 cm^{-1} and ~1075 cm^{-1}, assignable to ν(N-CSS) and ν_{assy} (CSS) stretching are suggestive of an anisobidentate chelation of the dithiocarbamate ligand.[24] Apart from this, two strong absorption bands appeared at ~ 570 and ~ 425 cm^{-1}, attributable to Sn-C and Sn-S stretching frequencies respectively. In the ^{1}H and ^{13}C NMR spectra of complexes **1-6**, signals corresponding to methine/methylene groups of N*CH*/*CH*$_2$-substituents and methylene group of N*CH*$_2$CO-linker, experience significant down-field displacements when compared to the respective diamino precursors. Notably complexes **1** and **2** display two peaks corresponding to NC*H*$_2$CO-linker hydrogen atoms due to different orientations of these groups in the binuclear macrocyclic complexes which is also reflected in the optimized structures. Importantly, ^{119}Sn NMR data provide valuable information about the structural details around the metal center. Despite the significant dependence of the chemical shift ranges of ^{119}Sn signals on the nature of the substituents, there is an approximate linear relationship between the ^{119}Sn

values and the coordination number of the complexes. For instance literature reports suggest ^{119}Sn NMR spectral ranges *viz* +200 to−60, −90 to−190, −210 to−400 and−440 to−540 ppm for four, five, six and seven coordination numbers of tin compounds, repectively.[27] All the complexes **1-6** display only one sharp singlet in range -236 to -242 ppm in their respective ^{119}Sn NMR spectra, suggestive of a single species with the hexa-coordinated tin centers.[25] Though self-assembly of a discrete supramolecular structure always proceed in competition with polymerization,[26] literature reports underline its dependency on the strereo-electronic features of ligand framework,[27] transition metal centers[28] as well as thermodynamic conditions.[27] It is anticipated that the formation binuclear diphenyltin^{IV}dithiocarbamate complexes based upon thermodynamic preference, profiting from enthalphic as well as entropic effects over oligomeric or polymeric species. The appearance of sharp signals with proper splitting patters and absence of signals for uncoordinated end groups in the NMR spectra of **1-6** ruled out the possibility of formation of oligomers or coordination polymeric products because in case of oligomers or coordination polymers multiple signals or broadening of NMR signals are expected due to the large size of the structure and conformational mobility within the polymetallic assembly. The UV-visible absorption spectra of $\mathbf{L^1}$-$\mathbf{L^6}$ exhibit a single prominent band at shorter wavelength ~300 nm, attributable to $\pi\rightarrow\pi^*$ (phenyl) transitions whereas binuclear complexes **1-6** show two principal bands at ~ 300 nm and at ~ 410 nm, attributable to $\pi\rightarrow\pi^*$ (phenyl) and charge transfer transitions, respectively, which is consistent with the absorption behavior of diorganotin dithiocarbamates.[29]

Among the ligand precursors, $\mathbf{L^1}$ and $\mathbf{L^3}$ exhibit higher emission intensity at 377 nm and 379 nm from locally excited $\pi\rightarrow\pi^*$ transition states, however the rest of the ligand precursors displayed weak emission intensity upon excitation at their respective λ_{max} values at room temperature. Expectedly the florescence property of diamine precursors $\mathbf{L^1}$-$\mathbf{L^6}$ (except $\mathbf{L^2}$) has been quenched upon the formation of respective binuclear complexes with Ph_2Sn^{IV}. This fluorescence quenching behavior of binuclear Ph_2Sn^{IV}dithiocarbamate complexes is consistent with the fluorescence behavior of flavonoid organotin^{IV} derivatives, which are reportedly fluorescent when they are pentacoordinate, but non-fluorescent when they are hexacoordinate.[30] A single/ multistage thermal degradation of the diamine precursors as well as binuclear complexes was observed on corresponding TG curves (Figure 1) which are indeed

accompanied by various endothermic and/or exothermic peaks DTA curves. The different temperatures exhibiting maximum rate of degradation for these compounds were recorded on DTG curves. Such a multistage thermal degradation pattern has previously been reported for a number of organotin^{IV}dithiocarbamate complexes.[31] TG curves demonstrate relatively greater thermal stability of binuclear diphenyltin^{IV}dithiocarbamates **1**, **2** and **6** than others. In all the cases, the weight loss continues till 550°C, except complex **3** which surprisingly exhibits a mass loss of 86.4% probably due to the formation of volatile products.[32]

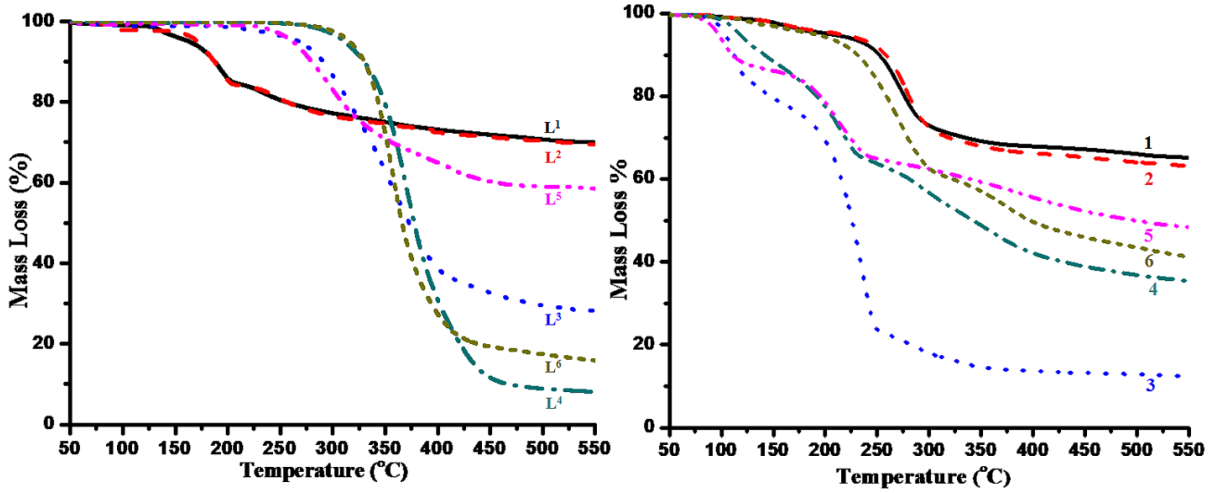

Figure 1. TG curves for diamine precursors **L^1-L^6** and binuclear diphenyltin^{IV}dithiocarbamate complexes **1-6**.

4.3.2. Computational Investigations

In order to obtain a better understanding of the spectroscopic results and to establish structure-property correlation, we performed full geometry optimizations of diamine precursors **L^1-L^6** (Annexure) and complexes **1-6** (Figure 2) using density functional theory (DFT) at B3LYP/6-31G (d, p) and B3LYP/LanL2DZ basis sets, respectively. The electronic structural parameters were found in good agreement with the X-ray data of closely related compounds.[33, 34]

An optimized geometry for **L^1-L^6** reveals the existence of *'gauche'* conformation of the phenyl rings adjacent to ethereal oxygen. The loss of coplanarity of amide moiety and significant deviations in the electronic structural parameters such as Ar-O-Ar dihedral angles in the binuclear complexes **1-6**, compared to diamino precursors, confirms the flexibility associated with the –$(CH_2CONHC_6H_5)_2O$– linker framework which could be an essential feature for effective interactions with biomolecules.

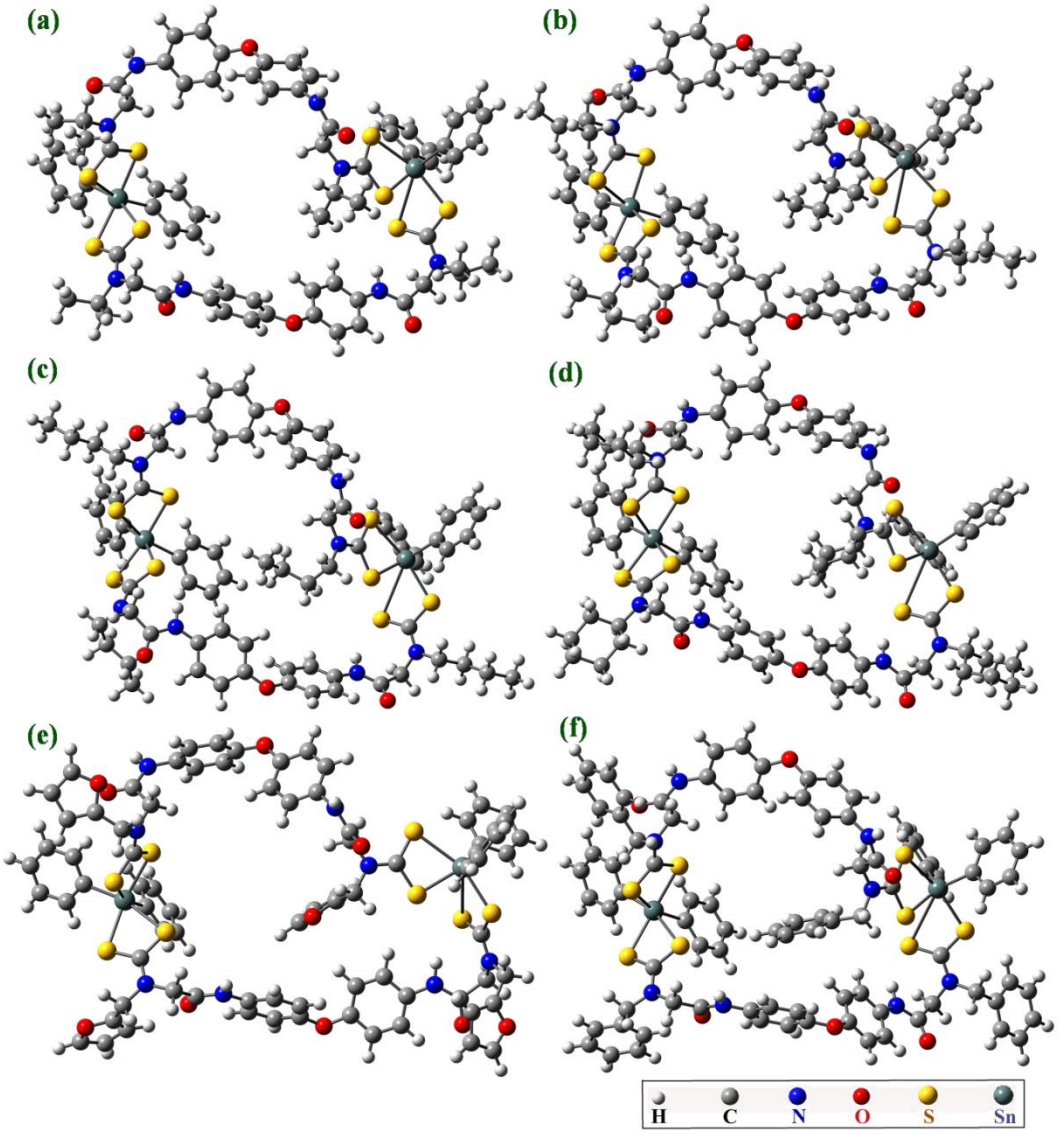

Figure 2. An optimized geometry for the minimum energy conformation at B3LYP/LanL2DZ level, (a): for complex **1**, (b): for **2**, (c): for **3**, (d): for **4**, (e): for **5** and (f): for **6**.

The optimized geometries of **1-6** clearly suggest that two ligand molecules bridges over two tin centers *via* chelating sites of terminal dithiocarbamate resulted into the formation of binuclear macrocyclic scaffolds having distorted octahedral geometry with *cis-cis* arrangement of diphenyltin moieties. One of the four *N*-alkyl substituents in the macrocyclic architecture is projected towards the inner side of the 44-member molecular cavity which can be visualized in the space-filling models of optimized geometries (Figure 3). The anisobidentate coordination mode of the -NCS_2 moieties is clearly reflected by the significant differences in the Sn–S bond distances (2.50-3.62 Å) and N–CS_2 bond distances (1.34–1.36 Å). The PhC–Sn–CPh bond angles associated with one of the Sn center are appeared in the range of 113.73-116.23 whereas the similar measurements associated with another Sn center are appeared in the range of

101.88-103.31° which is comparable to the experimental result.[34] A significant difference *viz.* 0.62, 2.81, 3.04, 2.87, 3.61 and 0.14° in the ethereal C-O-C bond angles of two linkers of 1-6 has been observed, respectively. The transannular Sn···Sn distances of 14.5, 13.8, 13.3, 14.5, 16.1 and 16.1 calculated for our 44-membered macrocycles **1-6**, respectively, are comparable to the similar distances obtained experimentally for other 33 member macrocycles,[11b,34] however these are significantly larger than those of analogous systems.[35] The accessible cavity size in **1-6** has been calculated from the closer transannular atoms which falls under the dimension of ≈6 × 11 $Å^2$ (Figure 3) and the macrocyclic cavity seems to be hydrophobic because of S atoms and *N*-alkyl substituent oriented inwards. The molecular electrostatic potential (MESP) of any chemical species provides valuable information about electronic environment of the molecule which is one of the essential factor for the prediction of its properties and potential sites for reactivity including biological systems and processes.[36] The mapping of electrostatic potential surface clearly shows the presence of slight negative potential around amide oxygen as well as positive potential around amide proton in complexes **1-6**. This suggests the potential accessibility of amide functionality as donor-acceptor sites for the hydrogen bonding interactions. The amide functionalities are arranged at the peripheral position of the cavity generated by macrocyclic architectures; however their different orientations are arises due the differences in their size and shape of the macrocyclic architectures which largely depends on the various *N*-alkyl substitutes. This generates a scope for fine tuning of reactivity profile of these macrocyclic receptors towards various guest molecules including biomolecules.

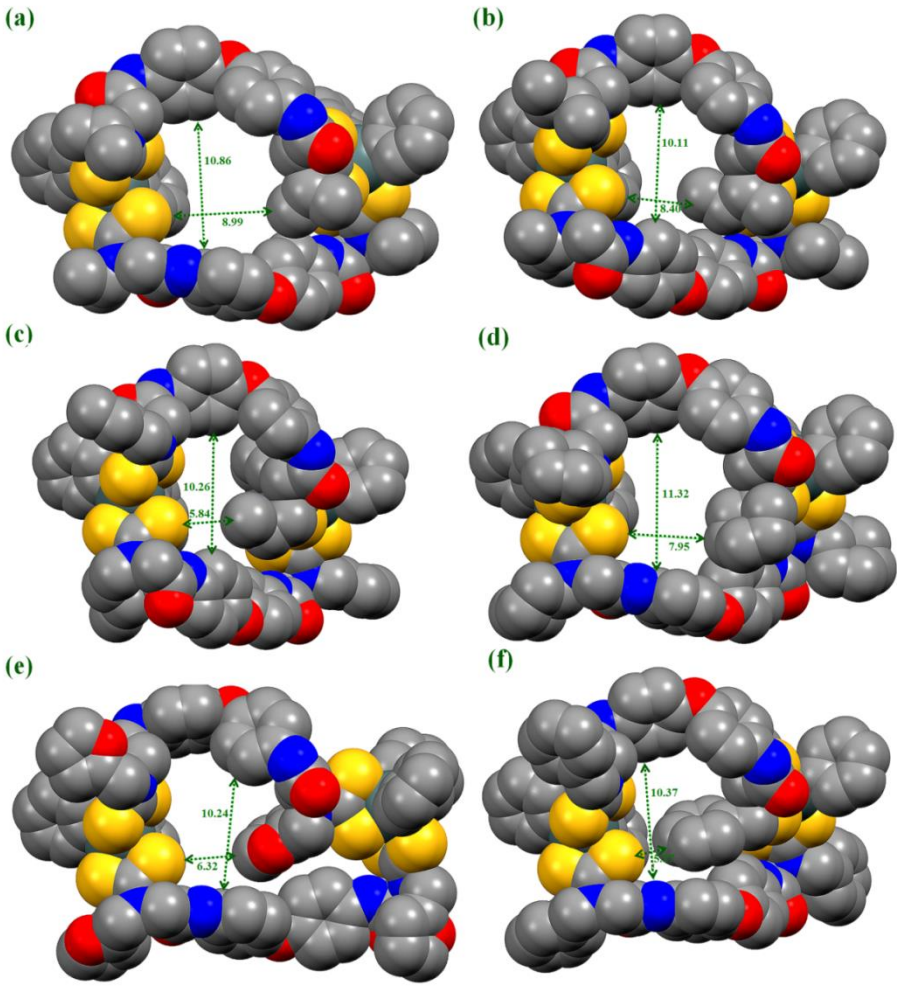

Figure 3. An optimized geometry in spacefilled model revealing cavity generated by macrocyclic architecture of dinuclear Ph_2Sn^{IV}dithiocarbamate complexes **1**; (a), **2**; (b), **3**; (c), **4**; (d), **5**; (e) and **6**; (f).

Moreover the nature of the frontier orbitals and the HOMO–LUMO energy gap greatly contribute to the photo-physical properties of the complexes, hence it becomes essential to analyse frontier molecular orbitals for prediction of the possible reactivity of the molecule.[37] The study suggests that the electron density of HOMO is localized over the phenyl rings adjacent to the ethereal oxygen of the one of the linker moiety in **1-6** while LUMO is predominantly localized at one of the diphenyltin^{IV}dithiocarbamate moiety. The calculated HOMO-LUMO energy differences for binuclear Ph_2Sn^{IV}dithiocarbamate complexes **1-6** falls in the range 3.6-4.1 eV, suggestive of the semiconducting nature of these compounds.[33] Generally, the authenticity of computational investigations is verified by the analogous experimental results; in this work the calculated HOMO-LUMO gaps for complexes **1-6** are clearly supported by their corresponding UV-visible absorption data showing comparable λ_{max} values.

4.3.3. In vitro cytotoxic activity

MTT Assay: All the new derivatives 4,4'-bis(2-chloroacetamido)diphenyl ether (**L'**), 4,4'-bis(2-(alkylamino)acetamido)diphenyl ethers (**L^1-L^6**) and binuclear Ph_2Sn^{IV}dithiocarbamate macrocyclic complexes (**1-6**) were screened for their possible anticancer activity by the MTT assay[22] against the malignant tumor cell lines Hep3B (Hepatoma) and IMR 32 (Neuroblastoma). For comparison purposes, the cytotoxic activity of diphenyltin dichloride and cisplatin (**R**) has also been evaluated under the same experimental conditions. The cytotoxicity observed for these compounds were compared with clinically used antineoplastic drug cisplatin. The 50% inhibition concentration (IC_{50}) values obtained after incubation of 14 h for all the compounds against both the cell lines are summarized in Table 1.

Table 1. In vitro cytotoxicity IC_{50} (μM) for the compounds under investigation.

Entry	Compound	Antitumor activity (IC_{50} values)	
		HEP 3B μM (1mL) ±SE	IMR 32 μM (1mL) ±SE
1[a]	4,4'-Diaminodiphenyl ether (**L[a]**)	415.4±2.15	272.423±2.40
2	4,4'-bis(2-chloroacetamido)diphenyl ether (**L'**)	4.78±0.23	7.45±0.34
3	**L^1**	21.76±0.25	39.15±2.76
4	**L^2**	20.28±0.49	29.66±1.36
5	**L^3**	10.13±0.35	14.35±1.48
6	**L^4**	8.25±0.75	38.23±2.93
7	**L^5**	11.17±0.51	20.23±2.21
8	**L^6**	12.37±0.61	13.77±1.82
9	**1**	4.40±0.13	4.25±0.67
10	**2**	4.50±0.11	4.31±0.33
11	**3**	3.83±0.12	5.69±0.64
12	**4**	2.88±0.08	3.12±0.47
13	**5**	3.00±0.12	3.46±0.29
14	**6**	3.76±0.09	6.10±1.16
15	Ph_2SnCl_2	12.66±0.64	14.04±3.12
16	Cisplatin (**R**)	56.47±3.93	61.90±5.19

([a]: IC_{50} value taken from ref 23; The data are expressed as μM concentration and value represents the average of three sets of independent experiments.)

The IC_{50} values clearly reveal that the entire groups of compounds exhibit higher cytotoxicity against both the cell lines, compared to **L[a]** and **R** (Figure 4). These compounds (except binuclear complexes **1** and **2**) display higher cytotoxic activity against HEP 3B compared to IMR 32 cell lines which is consistent with the trend shown by cisplatin. Interestingly, the presence of 2-chloroacetamido moiety at the terminal position of **L'** derivative, extensively increases the cytotoxic activity by 87 and 36 folds against HEP 3B (4.78±0.23 μM) and IMR 32 (7.45±0.34 μM) cell lines respectively, compared to the lead compound **L[a]**. This exceptional antitumor activity could be expected due to increased sites for hydrogen bonding and the presence of

highly vulnerable α-chloro moiety which make these molecules reactive towards biomolecules for nucleophilic substitution reactions. The substitution of α-chloro moiety with a variety of primary amines containing bulkier alkyl groups is expected to increase the lipophilic character of new derivatives **L^1-L^6** and thus their cytotoxicity. In contrast to this, their activity is rather decreased by 2-5 folds (8.25-21.76 μM against HEP 3B and 13.77-39.15 μM against IMR 32) and they fail to persevere the cytotoxic activity observed for **L'**.

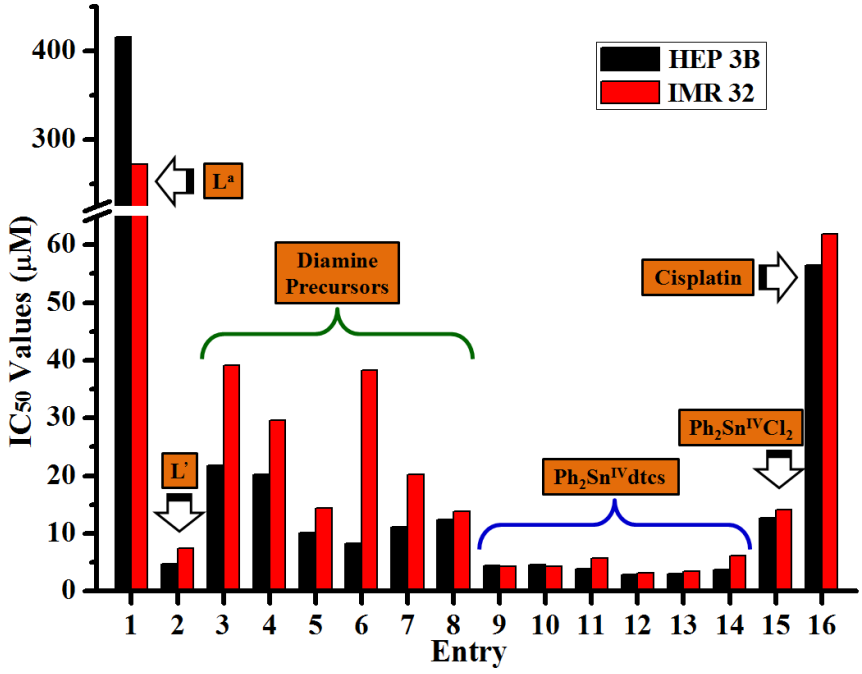

Figure 4. In vitro cytotoxicity for entries **1-16** (as per the Table 1) against HEP 3B and IMR 32 cancer cell lines.

Expectedly, the complexation of these derivatives **L^1-L^6** with biologically active Ph_2Sn^{IV} fragments enhances cytotoxic activity of binuclear Ph_2Sn^{IV}dithiocarbamate macrocyclic complexes **1-6** to a great extent, i.e. >2-5 fold enhancement in cytotoxicity is observed, compared to **L^1-L^6**. However all these scaffolds were found extremely active against both the cell lines and cytotoxicity data confirms the >12 fold better potency (for **1-6**) compared to cisplatin, a well known antineoplastic drug. The cytotoxicity of these complexes follows the order **4**>**5**>**6**>**3**>**1**>**2** against HEP 3B while this trend is changed to **4**>**5**>**1**>**2**>**3**>**6** against IMR 32. Notably, complex **4** bearing *N*-cyclohexyl substituents (IC_{50} values: 2.88±0.08 μM for HEP 3B and 3.12±0.47 μM for IMR 32) and complex **5** bearing *N*-(2-furfuryl) substituents (IC_{50} values: 3.00±0.12 μM for HEP 3B and 3.46±0.29 μM for IMR 32) exhibit optimum cytotoxicity. These

cytotoxicites are indeed more than 18-20 folds, compared to that of clinically used antineoplastic drug cisplatin.

The overall data suggest that all the derivatives exhibit better activity than the lead compound 4,4'-diaminodiphenyl ether, diphenyltin^{IV}dichloride and cisplatin, projecting them as more potent cytotoxic agents. Hence, a variation in the structural subunits of self assembly successfully implies the enhanced cytotoxic activity against HEP 3B and IMR 32 cell lines. (Figure 5) The derivatives **L'**, **L^1-L^6** and **1-6** can be ranked as good, moderate and excellent antitumor agents, respectively.

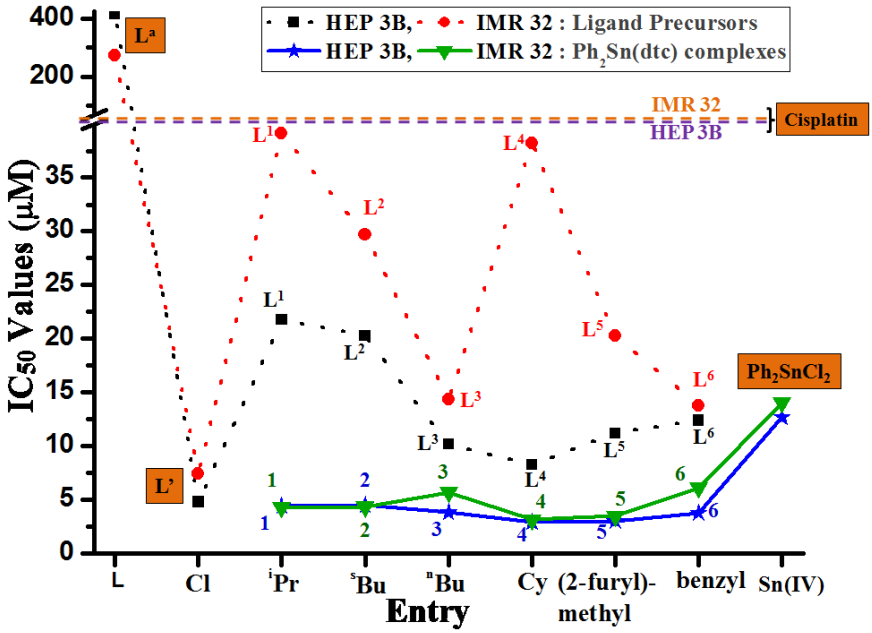

Figure 5. Effect of various *N*-alkyl substituents on the cytotoxicity against HEP 3B and IMR 32 cancer cell lines.

To establish structure-activity relationship (SAR), theoretical calculation is a one of the robust tool used now a day.[38] The structural and stereo-electronic parameters obtained from the theoretical calculation provide mechanistic insights associated with the transportation of molecules across the cell membranes, interactions of pharmacophores with biological macromolecules such as enzymes or intracellular receptors. For instance the energies of LUMO and HOMO-LUMO gap, reveal the stability and reactivity of the molecules towards potential biological receptors.[39] The dipole moment helps to understand the degree of lipophilicity of the molecules which indeed reveals the ability of the molecules to overcome biological barriers to move into different biofuels.[40] The extraordinary potency of binuclear complex **4** against both the cell lines can be clearly supported by highest LUMO energy (-1.2912 eV) and HUMO-

LUMO energy gap (4.02 eV) together with the greatest value of residual charges on Sn^{IV} (1.056 e.u).

Moreover the surface potential of the molecule also provides crucial information about the potential sites for non-covalent interactions with the biological targets, leading to effective cellular membrane transportation and hence increased concentration at the site of action. The surface potentials of the binuclear macrocyclic motifs **1-6** clearly demonstrates that the polar amide subunits are projected towards the peripheral side of the macrocyclic motifs that may provide H-bond acceptor (>C=O) and H-bond donor (>NH) sites and facilitate the interactions with biomolecules.

The literature reports suggest that DNA could be the probable target for the cytotoxic activity[41] of organotin compounds as these compounds can affect the primary structure of DNA and induces a complex, prolonged and variable response in cells which may lead to cell death via regulated apoptosis or necrosis is the alternatives.[42] Further the inhibition of macromolecular synthesis, mitochondrial energy metabolism, reduction of DNA synthesis and interaction with the cellular membrane which increases cytosolic Ca^{2+} concentration have been considered in organotin induced cytotoxicity.[43] Moreover, the diorganotin chlorides reportedly induce the apoptotic pathway which starts with an increase in the concentration of Ca^{2+} ions followed by the release of the cytochrome c from mitocondria, activation of caspases and finally DNA fragmentation.[44] It is anticipated that the binuclear Ph_2Sn^{IV}dithiocarbamate macrocyclic complexes **1-6** may exert their cytotoxic effects by involving these pathway(s). However the exact balance of the modes of action of these complexes may differ significantly from one cell type to another and among different organisms.

Apoptosis Studies: Apoptosis is a key process in higher organism. This is important for boy hemoostasis during development, embryonic development, the immune system, and ageing. The process also plays important role in many pathological conditios like cancer and neurodegeneration.[45] Apoptotic cell death is postulated to be the crucial mechanism in natural tumor suppression and cancer treatment, which eliminate abnormal malignant cells and reduce the tumor size.[46] It is important to develop novel chemical agents to specifically induce apoptosis for therapeutic purposes. Extension to MTT assay, the 'Flow cytometry' is considered as the analytical tool for investigation of potency, not only for cell viability, but also to evaluate membrane and chromosomal damage, cell-cycle analysis and morphological changes. Hence, for quantification of

extent of apoptotic and necrotic cell death, flow cytometry studies were performed upon treatment of some representative compounds on hepatocellular carcinoma HEP 3B and neuroblastoma IMR 32 cells. (Table 2) The flow-cytometric density plots (Figure 6) clearly evident the induction of apoptosis in HEP 3B and IMR 32 cells after treatment **L'**, **L^4**, **L^5**, binuclear Ph_2Sn^{IV}dithiocarbamate macrocyclic complexes **4** and **6**.

Table 2. Apoptotic/ necrotic population of HEP 3B and IMR 32 cells upon treatment of **L'**, **L^4**, **L^5**, binuclear Ph_2Sn^{IV}dithiocarbamate macrocycles **4**, **6**, **Control** and **Cisplatin**.

Sample	HEP 3B (%)				IMR 32(%)			
	Necrotic	Apoptotic	Live cells	Pro-apoptotic	Necrotic	Apoptotic	Live cells	Pro-apoptotic
L'	66.3	29.3	0.1	4.3	31.9	60.7	0.1	7.3
L^4	53.9	40.4	0.1	5.7	42.2	44.7	0.2	12.9
L^5	6.5	47.5	0.3	45.7	1.1	3.8	0.1	95.0
4	7.6	53.7	0.3	38.4	41.6	56.9	0.2	1.2
6	7.2	66.9	0.1	25.8	34.1	65.0	0.2	0.7
Control	0.1	0.0	99.8	0.1	0.1	0.0	99.7	0.2
Cisplatin	10.3	30.4	0.0	59.3	...	...	...	...

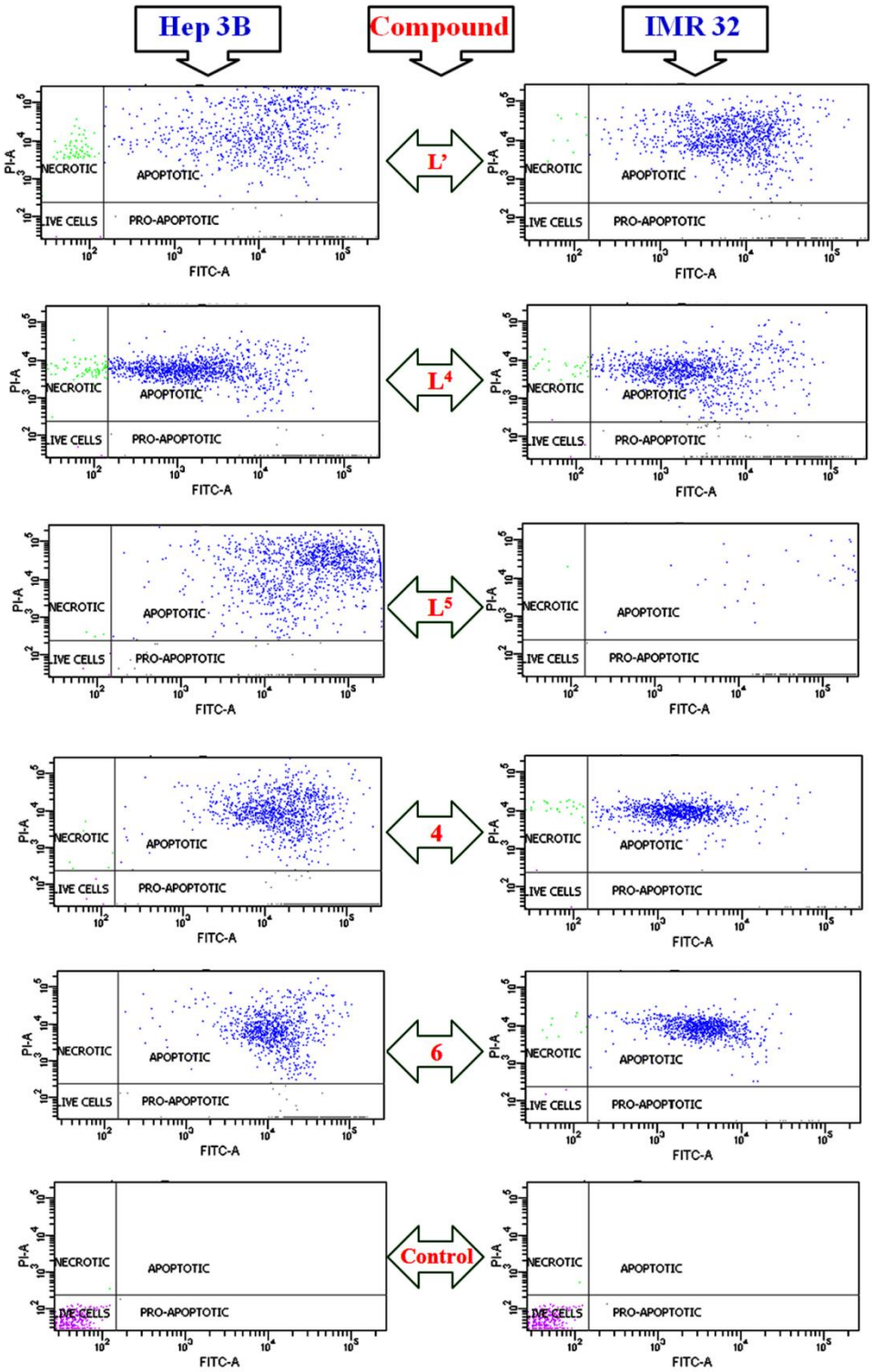

Figure 6. Flow cytometry density plots of HEP 3B and IMR 32 after the treatment of **L'**, **L**^{4}, **L**^{5}, binuclear Ph_2Sn^{IV}dithiocarbamate macrocyclic complexes **4** and **6**.

Importantly, both the cell lines display less than 0.3% live cell population after treatment with investigated compounds (Figure 7) and reinforced the extreme cytotoxicity of these compounds shown by MTT assay. All the investigated compounds display greater amount of apoptotic cell population in both the cell lines (except **L'** and

L^{4} against HEP 3B cells). Notably, HEP 3B and IMR 32 cells after treatment with binuclear Ph_2Sn^{IV}dithiocarbamate complexes **4** (53.7% HEP 3B; 56.9% IMR 32) and **6** (66.9% HEP 3B; 65.0% IMR 32) predominantly follow apoptotic cell death. The compound **L'** exerted necrosis significantly higher in HEP 3B (66.3% PI positive cells) than in case of IMR 32 (31.9 % PI positive cells) and this trend is consistent with **L**^{4}. The treatment of IMR 32 cells with diamino precursor **L**^{5}, gives very high (95%) proapoptotic cell populations. (Figure 7) The lower necrotic behavior of compounds **L**^{5}, **4** and **6** compared to cisplatin (Table 2) against HEP 3B cells, adds further merit to these compounds towards drug discovery.

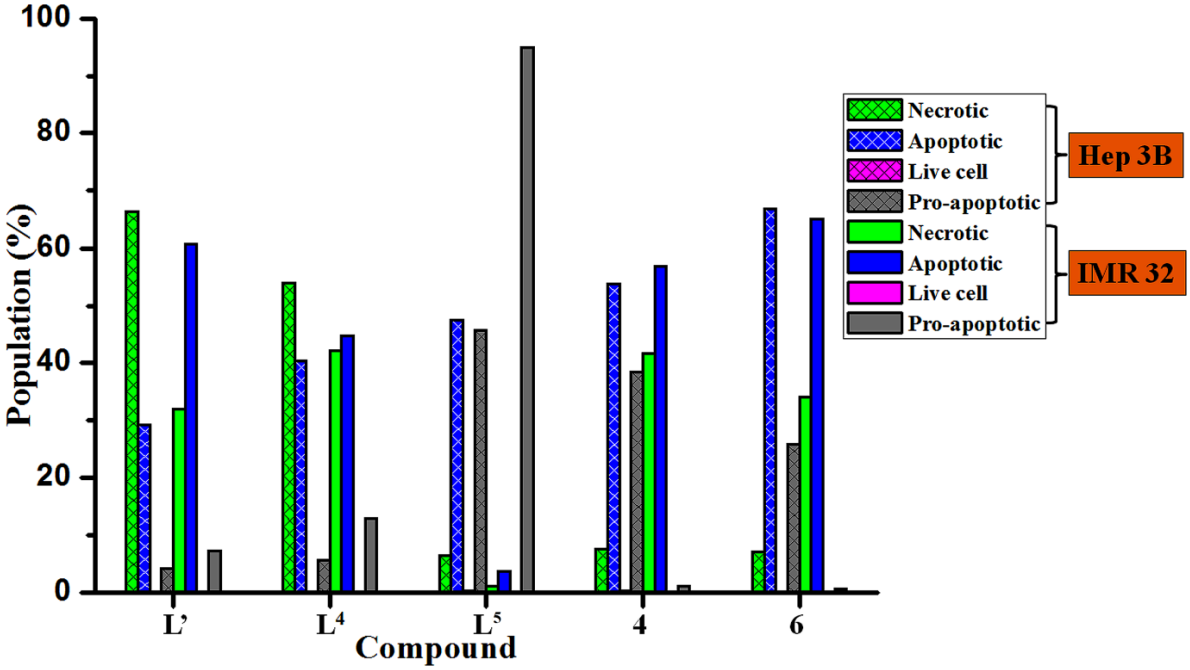

Figure 7. Apoptotic/ necrotic/ live cell populations of HEP 3B and IMR 32 cells upon treatment of **L'**, **L**^{4}, **L**^{5}, **4** and **6**.

Simultaneous binding of annexin V and propidium iodide in the cells treated with **L**^{4} (HEP 3B and IMR 32), **4** (IMR 32) and **6 (**IMR 32) is an indicative of the transition of apoptosis to necrosis (late apoptosis and secondary necrosis).[47] The selectivity associated with macrocyclic scaffolds **4** and **6** can be visualized by their distinct behavior against both the cell lines, reflected by larger population of sum of apoptotic and pro-apoptotic HEP 3B cells (92.1% for **4** and 92.7% for **6**), compared to that of IMR 32 cells (58.1% for **4** and 65.7% for **6**). Further, the differences in the apoptotic, pro-apoptotic and necrotic cell populations in HEP 3B and IMR 32 cells after treatment are suggestive of different reactivity profiles of the compounds under

investigation and reinforce the hypothesis (*vide supra*) of involvement of distinct cellular receptors in the cytotoxic activity.

4.4. Conclusions

In the search of potent chemical agents that can induce apoptosis in human cancer cells, a number of organic and organometallic scaffolds have been synthesized efficiently and characterized. To achieve further details, the molecular structures of **L^1-L^6** and **1-6** have been investigated by means of density functional calculations. The optimized structures reveal the presence of hexa-coordinated tin centers in the binuclear Ph_2Sn^{IV}dithiocarbamate complexes **1-6** which is consistent with the spectral data, especially ^{119}Sn NMR and fluorescence data. All the organometallic Ph_2Sn^{IV}dithiocarbamate complexes **1-6** exhibit significant in vitro antiproliferative activity against both HEP 3B and IMR 32 human cancer cell lines which is >12 fold higher than cisplatin, a drug used for clinical treatment in cancer chemotherapy. Among the compounds under investigation, the optimum potency of binuclear complex **4** against both the cell lines is appeared to be associated with its highest energy of LUMO and greatest value of residual charges on Sn^{IV} center. Compound **4** and **6** are appeared to be potent apoptosis inducer agents in human Hepatoma and Neuroblastoma cells. The ability to induce apoptosis has major therapeutic implication in cancer therapy. The compounds need further validation in animal model of different cancer for exploring its antimurogenic abilities. The ease of synthesis and interesting in vitro antitumor activity against human cancer cell lines, make the present series of organometallic binuclear Ph_2Sn^{IV}dithiocarbamate scaffolds as a promising new class of compounds for the future development of anticancer agents.

4.5. References

1. Crowe, A. J. *Metal Compounds in Cancer Therapy*. Fricker, S. P. Ed.; Chapman & Hall: London, 1994; pp. 147. (b) Pieper, T.; Borsky, K.; Keppler, B. K. *Top. Biol. Inorg. Chem.* **1999**, *1*, 171. (c) De Matos, N.; Marta R. P. *Quimica* **2002**, *85*, 61.
2. Kaluđerović, G. N.; Kommera, H.; H.-Hawkins, E.; Paschke, R.; G.-Ruiz, S. *Metallomics* **2010**, *2*, 419.
3. Crowe, A. J. *Drugs Fut.* 1987, *12*, 255.

4. (a) Hadjikakou, S. K.; Hadjiliadis, N. *Coord. Chem. Rev.* **2009**, *253*, 235. (b) Gielen, M. *Coord. Chem. Rev*. **1996**, *151*, 41. (c) Yang, P.; Guo, M. *Coord. Chem. Rev*. **1999**, *185-186*, 189. (d) Cardin, C. J.; Roy, A. *Inorg. Chim. Acta* **1985**, *107*, 57. (e) Singh, N.; Gupta, S.; Nath G. *Appl. Organometal. Chem.* **2000**, *14*, 484. (f) Jabbar, S.; Shahzadi, I.; Rehman, R.; Iqbal, H.; Qurat-ul-ain; Jamil, A.; Kousar, R.; Ali, S.; Shahzadi, S.; Choudhary, M. A.; Shahid, M.; Khan, Q. M.; Sharma, S. K.; Qanungo, K. *J. Coord. Chem*. **2012**, *65*, 572. (g) Nath, M.; Kompelli, N.; Roy, P.; Das, S. *International Journal of Medical, Health, Pharmaceutical and Biomedical Engineering* **2014**, 8, 436. (h) Manuaba, I. B. P. *Indo. J. Chem*., **2008**, *8*, 418. (i) Li, Y.-l.; Wang, Z.-w.; Guo, P. Tang, L. Ge, R.; Ban, S.-r.; Chai, Q.-y.; Niu, L.; Li, Q.-s. *J. Inorg. Biochem.* **2014**, *133*, 1. (j) Ferreira, I. P.; de Lima, G. M.; Paniago, E. B.; Rocha, W. R.; Takahashi, J. A.; Pinheiro, C. B.; Ardisson, J. D. *Polyhedron* **2014**, *79*, 161.
5. (a) Alama, A.; Tasso, B.; Novelli, F.; Sparatore, F. *Drug Discovery Today* **2009**, *14*, 500. (b) Sondhi, S. M.; Johar, M.; Singhal, N.; Dastidar, S. G.; Shukla, R.; Raghubir, R. *Monatsh. Chem.* **2000**, *131*, 511. (c) Kamal, A.; Kumar, B. A.; Arifuddin, M.; Dastidar, S. G. *Bioorg. Med. Chem.* **2003**, *11*, 5135. (d) Singh, Y.; Palombo, M.; Sinko, P. J. *Curr. Med. Chem.* **2008**, *15*, 1802. (e) Dubey, R.; Singh, P.; Singh, A. K.; Yadav, M. K.; Swati, D.; Vinayak, M.; Puerta, C.; Valerga, P.; Kumar, K. R.; Sridhar, B.; Tewari, A. K. *Cryst.Growth Des.* **2014**, *14*, 1347.
6. Faraglia, G.; Fregona, D.; Sitran, S.; Giovagnini, L.; Marzano, C.; Baccichetti, F.; Casellato, U.; Graziani, R. *J. Inorg. Biochem.* **2001**, *83*, 31.
7. Friebolin, W.; Schilling, G.; Zöller, M.; *J. Med. Chem.* **2005**, *48*, 7925.
8. Warburg, O. *U¬ ber den Stoffwechsel der Tumoren*; Springer: Berlin, 1926.
9. (a) Lai, S. W.; Drew, M. G. B.; Beer, P. D. *J. Organomet. Chem.* **2001**, *637*, 89. (b) Beer, P. D.; Berry, N. Drew, M. G. B.; Fox, O. D.; P.-Tosta, M. E.; Patell, S. *Chem. Commun.* **2001**, 199. (c) Wong, W. W. H.; Curiel, D.; Cowley, A. R.; Beer, P. D. *Dalton Trans.* **2005**, 359. (d) Wong, W. W. H.; Cookson, J.; Evans, E. A. L.; Mc Innes, E. J. L.; Wolowska, J.; Maher, J. P.; Bishop, P.; Beer, P. D. *Chem. Commun.* **2005**, 2214. (e) Cookson, J.; Beer, P. D. *Dalton Trans.* **2007**, 1459.
10. (a) Menezes, D. C.; de Lima, G. M.; Carvalho, F. A.; Coelho, M. G.; Porto, A. O.; Augusti, R.; Ardisson, J. D. *Appl. Organometal. Chem.* **2010**, *24*, 650. (b) Barone, G.; Chaplin, T.; Hibbert, T. G.; Kana, A. T.; Mahon, M. F.; Molloy, K. C.; Worsley, I. D.; Parkin I. P.; Price, L. S. *J. Chem. Soc., Dalton Trans*. **2002**, 1085. (c) S.-Juarez, A.;

Ortiz, A.; *J. Electrochem. Soc.* **2000**, *147*, 3708. (d) Gou, X. L.; Chen, J.; Shen, P. W. *Mat. Chem. Phys.* **2005**, *93*, 557. (e) Kana, A. T.; Hibbert, T. G.; Mahon, M. F.; Molloy, K. C.; Parkin, I. P.; Price, L. S. *Polyhedron* **2001**, *20*, 2989.

11. (a) Tiekink, E. R. T. *CrystEngComm* **2003**, *5*, 101. (b) Tiekink, E. R. T. *Appl. Organomet. Chem.* **2008**, *22*, 533. (c) Awang, N.; Baba, I.; Yousof, N. S. A. M.; Kamaludin, N. F. *Am. J App. Sci.* **2010**, *7*, 1047. (d) Adli, H. K.; Sidek, N. M.; Ismail, N.; Khairul, W. M. *Chiang Mai J. Sci.* **2013**, 40, 117. (e) Singh, N.; Gupta, S.; Nath, G. *Appl. Organometal. Chem.* **2000**, *14*, 484. (f) Menezes, D. C.; Vieira, F. T.; de Lima, G. M.; Wardell, J. L.; Cort´es, M .E.; Ferreira, M. P.; Soares, M. A.; Boas, A. V. *Appl. Organometal. Chem.* **2008**, *22*, 221.
12. (a) T.-Huerta, A.; R.-Molina, B.; Höpfl, H.; G.-Garibay, M. A. *Organometallics* **2014**, *33*, 354. (b) Tlahuext, H.; R-Martínez, R.; V-Pineda, G.; L.-Cardoso, M.; Höpfl, H. *J. Organomet. Chem.* **2011**, *696*, 693. (c) S.-Juarez, E.; C.-Huerta, J.; H.-Ahuactzi, I. F.; R.-Martınez, R.; Tlahuext, H.; M.-Rojas, H.; Hopfl, H. *Inorg. Chem.* **2008**, *47*, 9804.
13. (a) Rao, C. N. R.; Natarajan, S.; Vaidhyanathan, R. *Angew. Chem., Int. Ed.* **2004**, *43*, 1466. (b) Ferey, C.; M.-Draznieks, C; Serre, C.; Millange, F. *Acc. Chem. Res.* **2005**, *38*, 217. (c) Hosseini, M. W. *Acc. Chem. Res.* **2005**, *38*, 313. (d) Nitschke, J. R. *Acc. Chem. Res.* **2007**, *40*, 103. (e) Pitt, M. A.; Johnson, D. W. *Chem. Soc. Rev.* **2007**, *36*, 1441. (f) Thomas, J. A. *Chem. Soc. Rev.* **2007**, *36*, 856. (g) Ariga, K.; Hill, J. P.; Lee, M. V.; Vinu, A.; Charvet, R.; Acharya, S. *Sci. Technol. Adv. Mater.* **2008**, *9*, 014109 (96 pp).
14. Cougnon, F. B. L. Sanders, J. K. M. *Acc. Chem. Res.* **2012**, *45*, 2211.
15. (a) Caulder, D. L.; Raymond, K. N. *Acc. Chem. Res.* **1999**, *32*, 975. (b) Seidel, S. R.; Stang, P. J. *Acc. Chem. Res.* **2002**, *35*, 972. (c) Fujita, M.; Tominaga, M.; Hori, A.; Therrien, B. *Acc. Chem. Res.***2005**, *38*, 369.
16. (a) Haiduc, I.; Edelmann, F. T. *Supramolecular Organometallic Chemistry*; Wiley-VCH, 2000. b) Chandrasekhar, V.; Nagendran, S.; Baskar, V. *Coord. Chem. Rev.* **2002**, *235*, 1. (c) Chandrasekhar, V.; Gopal, K.; Thilagar, P. *Acc. Chem. Res.* **2007**, *40*, 420.
17. (a) Giovagnini, L.; Ronconi, L.; Aldinucci, D.; Lorenzon, D.; Sitran, S.; Fregona, D. *J. Med. Chem.* **2005**, *48*, 1588. (b) Milacic, V.; Chen, D.; Ronconi, L.; L.-Piwowar, K. R.; Fregona, D.; Dou, Q. P. *Cancer Res.* **2006**, *66*, 10478. (c) V.-Rhenals, M.; Rieber, M. S.; Rieber, M. *Biochem. Pharmacol.* **2007**, *74*, 841. (d) Saggioro, D.; Rigobello, M. P.; Paloschi, L.; Folda, A.; Moggach, S. A.; Parsons, S.; Ronconi, L.; Fregona, D.; Bindoli, A. *Chem. Biol.* **2007**, *14*, 1128. (e) Chen, D.; Cui, Q. Z. C.; Yang, H. J.; Dou, Q. P.

Cancer Res. **2006**, *66*, 10425. (f). Cvek, B.; Milacic, V.; Taraba, J.; Dou, Q. P. *J. Med. Chem.* **2008,** *51*, 6256.

18. (a) Farrell, N.; Almeida, S. G.; Skov, K. A. *J. Am. Chem. Soc.* **1988**, *110*, 5018. (b) Pratesi, G.; Perego, P.; Polizzi, D.; Righetti, S. C.; Supino, R.; Caserini, C.; Manzotti, C.; Giuliani, F. C.; Pezzoni, G.; Tognella, S.; Spinelli, S.; Farrell, N.; Zunino, F. *Br. J. Cancer* **1999**, *80*, 1912. (c) Farrell, N.; Qu, Y.; Feng, L.; Van Houten, B. *Biochemistry* **1990**, *29*, 9522. (d) Skov, K. A.; Adomat, H.; Farrell, N.; Matthews, J. B. *Anti-Cancer Drug Des.* **1998**, *13*, 207. (e) Qu, Y.; Farrell, N. *Inorg. Chem.* **1992**, *31*, 930. (f) Davies, M. S.; Cox, J. W.; Berners-Price, S. J.; Barklage, W.; Qu, Y.; Farrell, N. *Inorg. Chem.* **2000**, *39*, 1710. (g) Farrell, N.; Appleton, T. G.; Qu, Y.; Roberts, J. D.; Fontes, A. P. S.; Skov, K. A.; Wu, P.; Zou, Y. *Biochemistry* **1995**, *34*, 15480. (h) Rauter, H.; Domenico, R.; Menta, E.; Oliva, A.; Qu, Y.; Farrell, N. *Inorg. Chem.* **1997**, *36*, 3919. (i) McGregor, T. D.; Hegmans, A.; Kaspárková, J.; Neplechová, K.; Nováková, O.; Penazová, H.; Vra´na, O.; Brabec, V.; Farrell, N. *J. Biol. Inorg. Chem.***2002**, *7*, 397. (j) Perego, P.; Caserini, C.; Gatti, L.; Carenini, N.; Romanelli, S.; Supino, R.; Colangelo, D.; Viano, I.; Leone, R.; Spinelli, S.; Pezzoni, G.; Manzotti, C.; Farrell, N.; Zunino, F. *Mol. Pharmacol.* **1999**, *55*, 528. (k) Teixeira, L. J.; Seabra, M.; Reis, E.; da Cruz, M. T. G.; de Lima, M. C. P.; Pereira, E.; Miranda, M. A.; Marques, M. P. M. *J. Med. Chem.* **2004,** *47*, 2917.
19. Zaludová, R.; Zakovská, A.; Kaspárková , J.; Balcarová, Z.; Kleinwachter, V.; Vrána, O.; Farrell, N.; Brabec, V. *Eur. J. Biochem.* **1997**, *246*, 508.
20. (a) Perego, P.; Gatti, L.; Caserini, C.; Supino, R.; Colangelo, D.; Leone, R.; Spinelli, S.; Farrell, N.; Zunino, F. *J. Inorg. Biochem.* **1999**, *77*, 59. (b) Farrell, N.; Qu, Y.; Hacker, M. P*J. Med. Chem.* **1990**, *33*, 2179. (c) Jansen, B. A. J.; Van der Zwan, J.; Reedijk, J.; Den Dulk, H.; Brouwer, J. *Eur. J. Inorg. Chem.* **1999**, 1429. (d) Farrell, N. *Cancer Invest.* **1993**, *11*, 578.
21. (a) Ito, H.; Kusukawa, T.; Fujita, M. *Chem. Lett.* **2000**, *29*, 598. (b) Cacciapaglia, R.; Stefano, S. D.; Mandolini, L. *Acc. Chem.Res.* **2004**, *37*, 113. (c) Fiedler, D.; Leung, D. H.; Bergman, R. G.; Raymond, K. N. *Acc. Chem. Res.* **2005**, *38*, 349. (d) Pluth, M. D.; Bergman, R. G.; Raymond, K. N. *Acc. Chem. Res.* **2009**, *42*, 1650. (e) Corma, A.; García, H.; L-Xamena, F. X. *Chem. Rev.* **2010**, *110*, 4606. (f) Fujita, M. *Chem. Soc. Rev.* **1998**, *27*, 417. (g) Hawthorne, M. F.; Zheng, Z. *Acc. Chem. Res.* **1997**, *30*, 267. (h) Beer, P. D.; Gale, P. A. *Angew. Chem., Int. Ed.* **2001**, *40*, 486. (i) Chen, B.; Xiang, S.;

Qian, G. *Acc. Chem. Res.* **2010**, *43*, 1115. (j) Beer, P. D. *Acc. Chem. Res.* **1998**, *31*, 71. (k) E.-Aroussi, B.; Guénée, L.; Pal, P.; Hamacek, J. *Inorg. Chem.* **2011**, *50*, 8588.

22. Manosroi, J.; Dhumtanom, P.; Manosroi, A. *Cancer Lett.* **2006**, *235*, 114.
23. Singh, V. K.; Kadu, R.; Roy, H. *Eur. J. Med. Chem.* **2014**, *74*, 552.
24. Reyes-Martínez, R.; Mejia-Huicochea, R.; G.-Alvarez, J. A.; Höpfl, H.; Tlahuext, H. *ARKIVOC* **2008**, *v*, 19.
25. (a) Dias, Letícia C.; Rubinger, M. M. M.; Barolli, J. P.; Ardisson, J. D.; Mendes, I. C.; Lima, G. M.; Zambolim, de L.; Oliveira, M. R.L. *Polyhedron* **2012**, *47*, 30. (b) Yousefi, M.; Safari, M.; Torbati, M. B.; Kazemiha, V. M.; Sanati H.; Amanzadeh, A. *Appl. Organometal. Chem.* **2012**, *26*, 438. (c) Sedaghat, T.; Goodarzi, K. *Phosphorus, Sulfur, and Silicon*, **2007**, *182*, 2227. (d) R.-Martínez, R.; García, P. G.; L.-Cardoso, M;. Höpfl, H.; Tlahuext, H. *Dalton Trans*., **2008**, 6624.
26. Ercolani, G. *J. Phys. Chem. B* **2003**, *107*, 5052.
27. Leininger, S.; Olenyuk, B.; Stang, P. J. *Chem. Rev*. **2000**, *100*, 853.
28. Jones, C. J. *Chem. Soc. Rev*. **1998**, *27*, 289.
29. (a) Singh, H. L.; Varshney, A. K., *Chem. Appl.*, **2006**; 1. (b) Barba, V.; Arenaza, B.; Guerrero, J.; Reyes, R. *Heteroatom. Chemistry*, **2012**, 23, 422. (c) F.-Martinez, J. P.; T.-Martinez, I.; R.-Bravo, P.; Garcia, P. G.; G.-Alcantar, C.; L.-Cardoso, M.; M.-Rojas H. *Polyhedron*, **2009**, *28*, 3953.
30. (a) V.-Ramos, R.; Yatsimirsky, A. K. *Chem. Commun*. **2011**, *47*, 2694. (b) Blunden, S. J.; Smith, P. J. *J. Organomet. Chem*. **1982**, *226*, 157.
31. (a) Sharma, R.; Kaushik, N. K. *J. Therm. Anal Calorim.* **2004**, *78*, 953. (b) Husain, A.; Nami, S. A.A.; Siddiqi, K. S. *Spectrochim. Acta Part A* **2009**, *73*, 89.
32. Tessier, E.; Amouroux, D.; Donard O. F. X. *Biogeochemistry* **2002**, *59*, 161.
33. Kadu, R.; Singh, V. K.; Verma, S. K.; Raghavaiah, P.; Shaikh M. M. *J Mol. Struct*. **2013**, *1033*, 298.
34. (a) Celis, N. A.; V.-Ramos, R.; Höpfl, H.; H.-Ahuactzi, I. F.; Sánchez, M.; Z.-Rivera, L. S.; Barba, V. *Eur. J. Inorg. Chem*. **2013**, *16*, 2912. (b) Tiekink, E. R. T. *Appl. Organomet. Chem.* **2008**, *22*, 533.
35. (a) C.-Huerta, J.; C.-Morales, M.; S.-Juárez, E.; H.-Ahuactzi, I. F.; E.-García, J.; G.-Alcantar, C.; G.-Alvarez, J. A.; Höpfl, H.; M.-Rojas, H.; Sánchez, M. *Inorg. Chem.* **2008**, *47*, 9874. (b) Altmann, R.; Gausset, O.; Horn, D.; Jurkschat, K.; Schürmann, M. *Organometallics* **2000**, *19*, 430.

36. (a) Gadre, S. R.; Bhadane, P. K. *Resonance*, **1999**, *4*, 8-19. (b) Bulat, F. A.; T.-Labbé, A.; Brinck, T.; Murray, J. S.; Politzer, P. *J Mol Model* **2010**, *16*, 1679. (c) Politzer, P.; Laurence, P. R.; Jayasuriya, K. *Environ. Health Perspect.* **1985**, *61*, 191.
37. Vladimirova, K. G.; Freidzon, A. Y.; Kotova, O. V.; Vaschenko, A. A.; Lepnev, L. S.; Bagatur'yants, A. A.; Vitukhnovskiy, A. G.; Stepanov, N. F.; Alfimov M. V. *Inorg. Chem.*, **2009**, *48*, 11123.
38. Ferreira, I. P.; de Lima, G. M.; Paniago, E. B.; Rocha, W. R.; Takahashi, J. A.; Pinheiro, C. B.; Ardisson, J. D. *Eur. J. Med. Chem.* **2012**, *58*, 493.
39. (a) Orr, S. T. M.; Ripp, S. L.; Ballard, T. E.; Henderson, J. L.; Scott, D. O.; Obach, R. S.; Sun, H.; Kalgutkar, A. S. *J. Med. Chem.* **2012**, *55*, 4896. (b) Parrilha, G. L.; da Silva, J. G.; Gouveia, L. F.; Gasparoto, A. K.; Dias, R. P.; Rocha, W. R.; Santos, D. A.; Speziali, N. L.; Beraldo, H. *Eur. J. Med. Chem.* **2011**, *46*, 1473. (c) Soares, M. A.; Lessa, J. A.; Mendes, I. C.; Da Silva, J. G.; dos Santos, R. G.; Salum, L. B.; Daghestani, H.; Andricopulo A. D.; Day, B. W.; Vogt, A.; Pesquero, J. L.; Rocha, W. R.; Beraldo, H. *Bioorg. Med. Chem*. **2012**, *20*, 3396.
40. Hansch, C.; Bonavida, B.; Jazirehi, A. R.; Cohen, J. J.; Milliron, C.; Kurup, A. *Bioorg. Med. Chem.* **2003**, *11*, 617.
41. (a) Boualam, M.; Willem, R.; Biesemans, M.; Gielen, M. *Appl. Organometal. Chem.* **1991**, *5*, 497. (b) Gielen, M.; Clercq, L. D.; Willem, R.; Joosen, E. in: J. J. Zuckerman (Ed.), *Tin and Malignant Cell Growth*, CRC Press, Boca Raton, PC, 1988, pp.39.
42. Pellerito, C.; Nagy, L.; Pellerito, L.; Szorcsik, A. *J Organomet. Chem.* **2006**, *691*, 1733.
43. (a) Aw, T. Y.; Nicotera, P.; Manzo, L.; Orrenius, S. *Arch Biochem Biophys* **1990** *283*, 46. (b) Viviani, B.; Rossi, D.; Chow, S. C.; Nicotera, P. *Toxicol Appl Pharmacol* **1996** *140*, 289. (c) Pizarro, A. M.; Habtemariam, A.; Sadler, P. J. *Top Organomet. Chem.* **2010**, *32*, 21.
44. (a) Gennari, A.; Bleumink, R.; Vivani, B.; Galli, C. L.; Marinovich, M.; Pieters, R.; Corsini, E.; *Toxicol. Appl. Pharmacol*. **2000**, *169*, 185. (b) Pellerito, C.; Nagy, L.; Pellerito, L. *J. Organomet. Chem.* **2006**, *691*, 1761.
45. (a) Jiang, W.; Fu, Y.; Yang, F.; Yang, Y.; Liu, T.; Zheng, W.; Zeng, L.; Chen T. *ACS Appl. Mater. Interfaces* **2014**, *6*, 13738. (b) Kim, G.; Kim, W.; Kim, K.; Lee, J. *Appl. Phys. Lett*. **2010**, *96*, 021502.
46. (a) Wlodkowic, D.; Faley, S.; Zagnoni, M.; Wikswo, J. P.; Cooper, J. M. *Anal. Chem.* **2009**, *81*, 5517. (b) Wlodkowic, D.; Skommer, J.; Darzynkiewicz, Z. *Cytometry, Part A*

2008, *73*, 496. (c) Hanahan, D.; Weinberg, R. A. *Cell* **2000**, *100*, 57. (d) Wlodkowic, D.; Skommer, J.; Faley, S.; Darzynkiewicz, Z.; Cooper, J. M. *Exp. Cell Res.* **2009**, *315*, 1706.

47. (a) Oltmanns, D.; Z.-Kolbe, S.; Mueller, A.; B.-Wuest, U.; Schaefer, M.; Eder, M.; Haberkorn, U.; Eisenhut, M. *Bioconjugate Chem*. **2011**, *22*, 2611. (b) Blume, K. E., Soeroes, S., Waibel, M., Keppeler, H., Wesselborg, S., Herrmann, M., Schulze-Osthoff, K., Lauber, K. *J. Immunol.* **2009**, *183*, 8138.

4.6. Annexure

4.6.1. Spectroscopic data

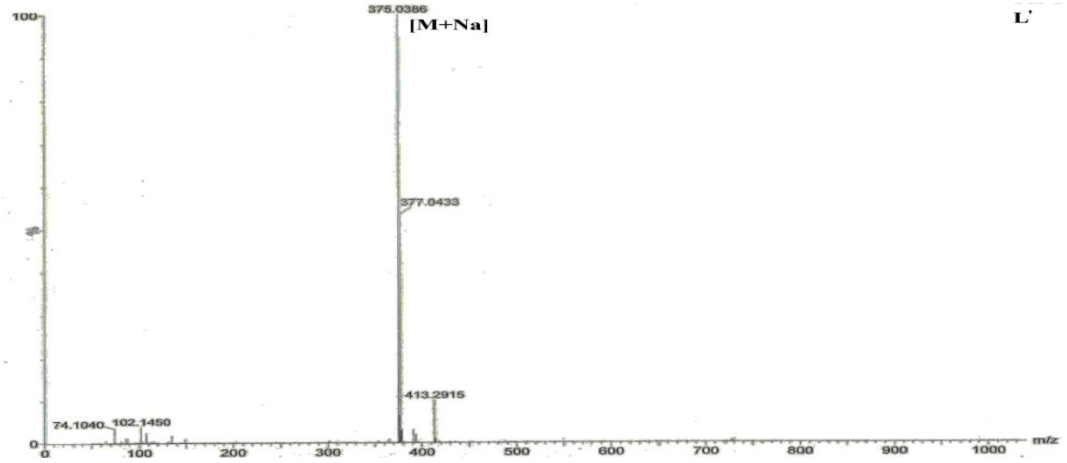

Annexure 1. Mass spectrum of **L'**.

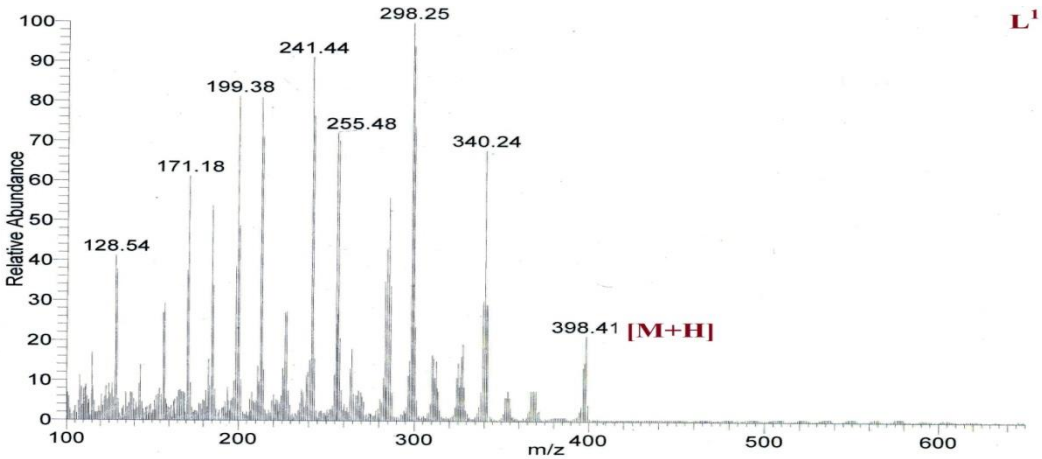

Annexure 2. Mass spectrum of **L**[1].

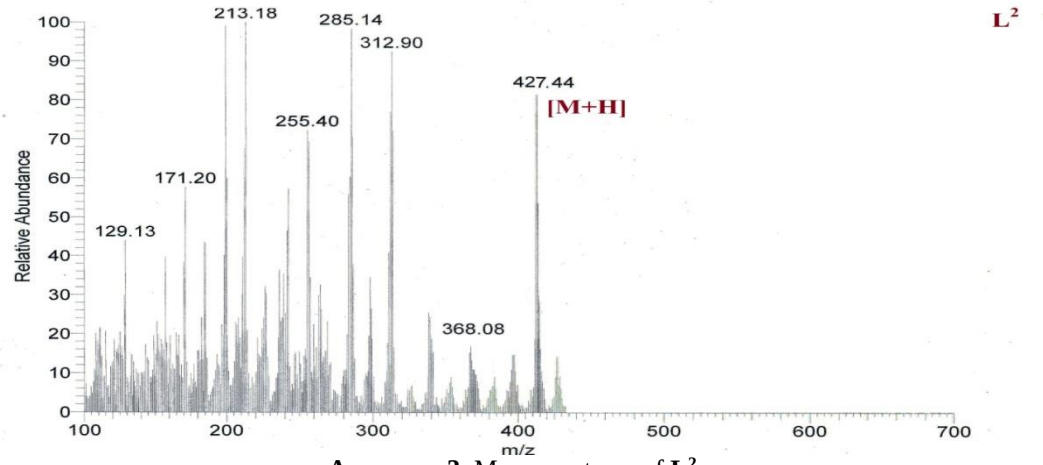

Annexure 3. Mass spectrum of **L²**.

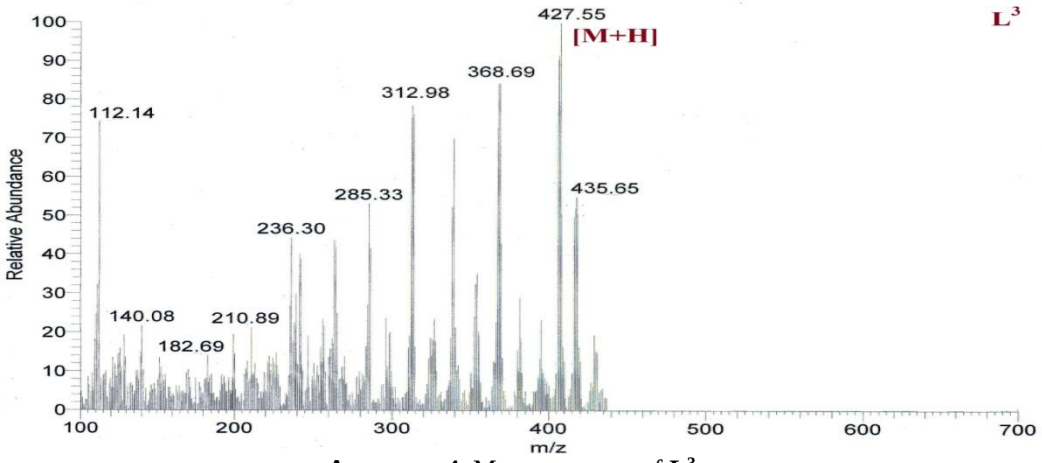

Annexure 4. Mass spectrum of **L³**.

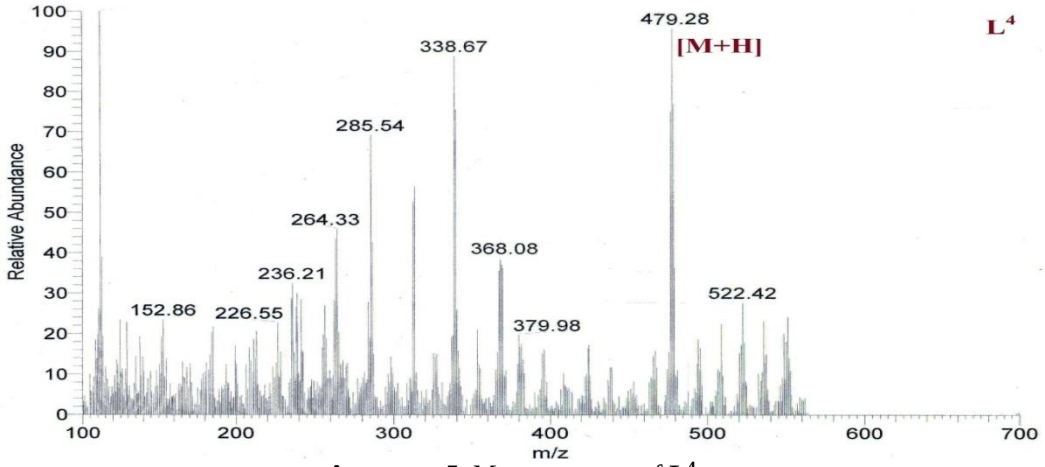

Annexure 5. Mass spectrum of **L⁴**.

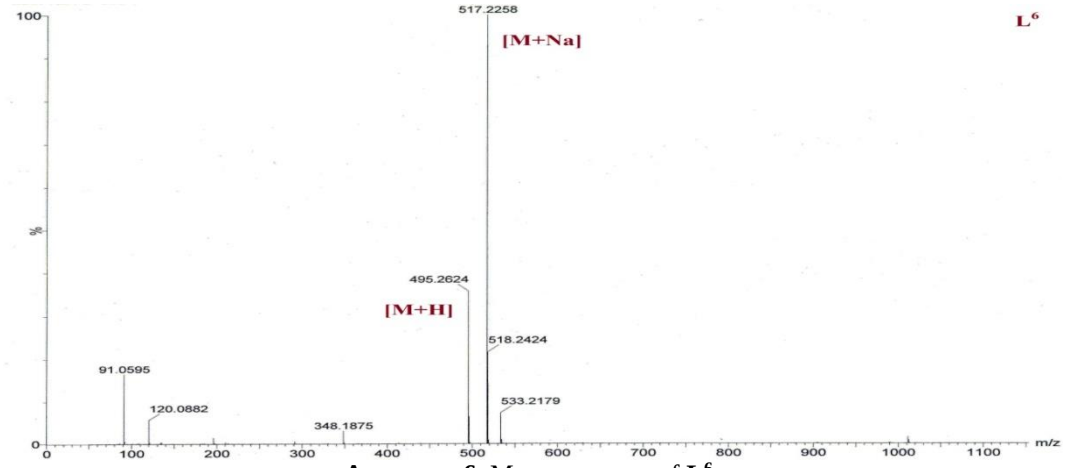

Annexure 6. Mass spectrum of **L^6**.

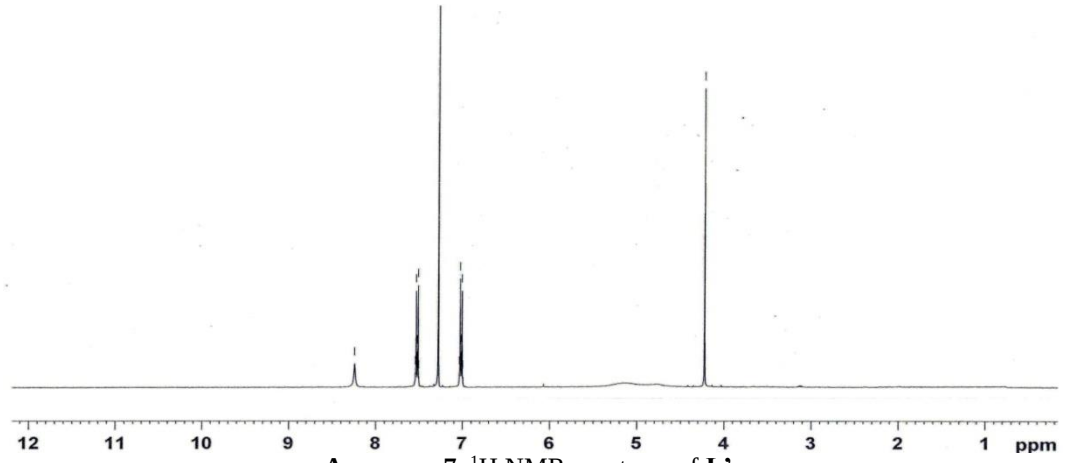

Annexure 7. ^{1}H NMR spectrum of **L'**.

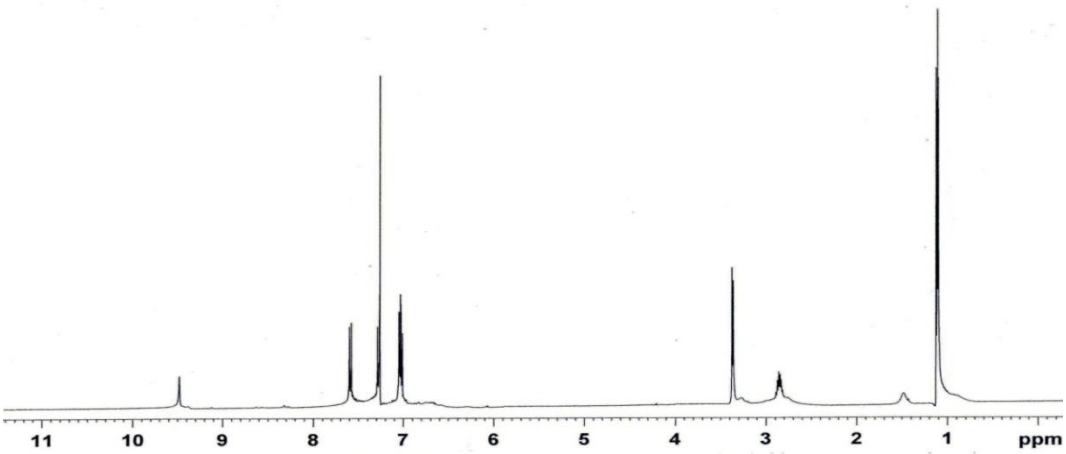

Annexure 8. ^{1}H NMR spectrum of **L^1**.

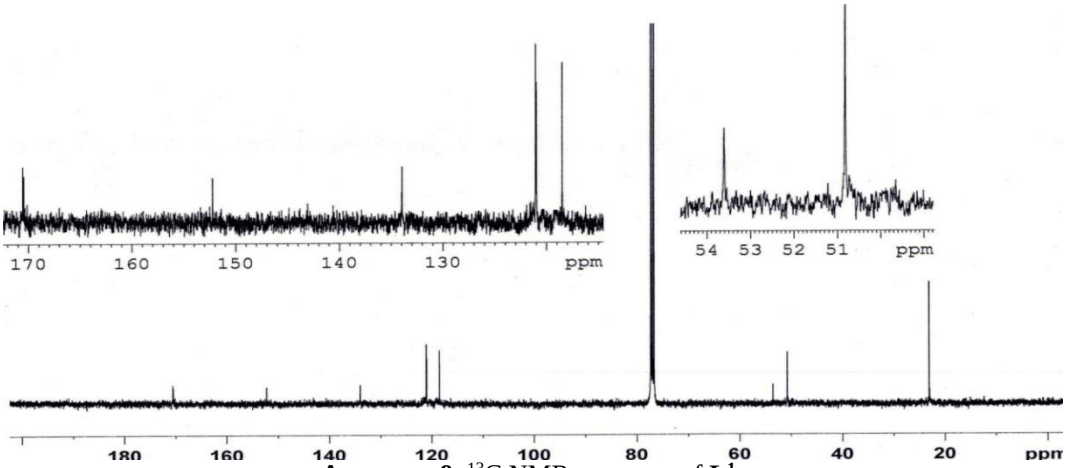

Annexure 9. ^{13}C NMR spectrum of $\mathbf{L^1}$.

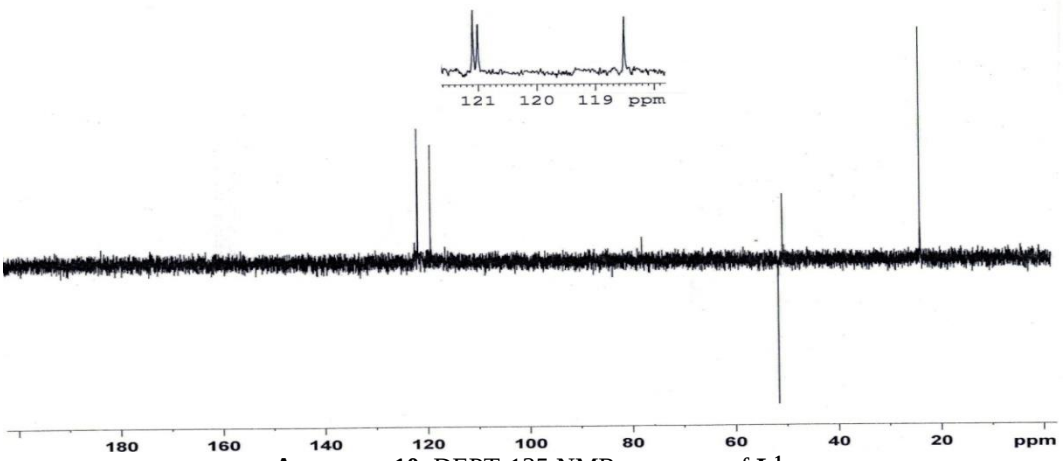

Annexure 10. DEPT-135 NMR spectrum of $\mathbf{L^1}$.

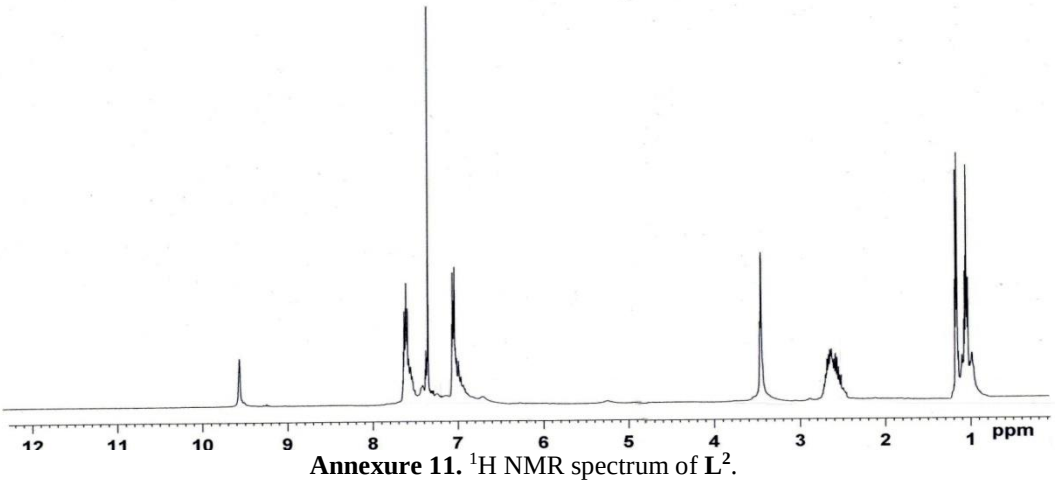

Annexure 11. ^{1}H NMR spectrum of $\mathbf{L^2}$.

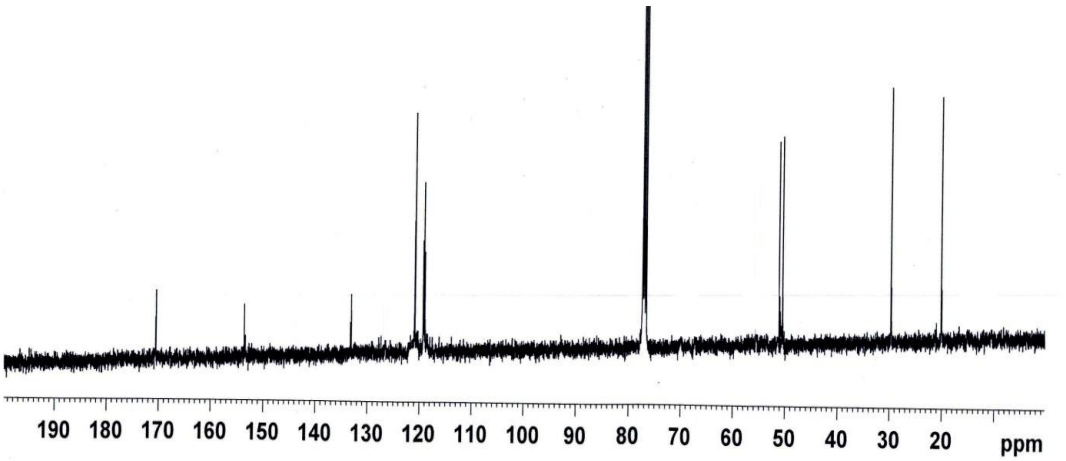

Annexure 12. ^{13}C NMR spectrum of **L²**.

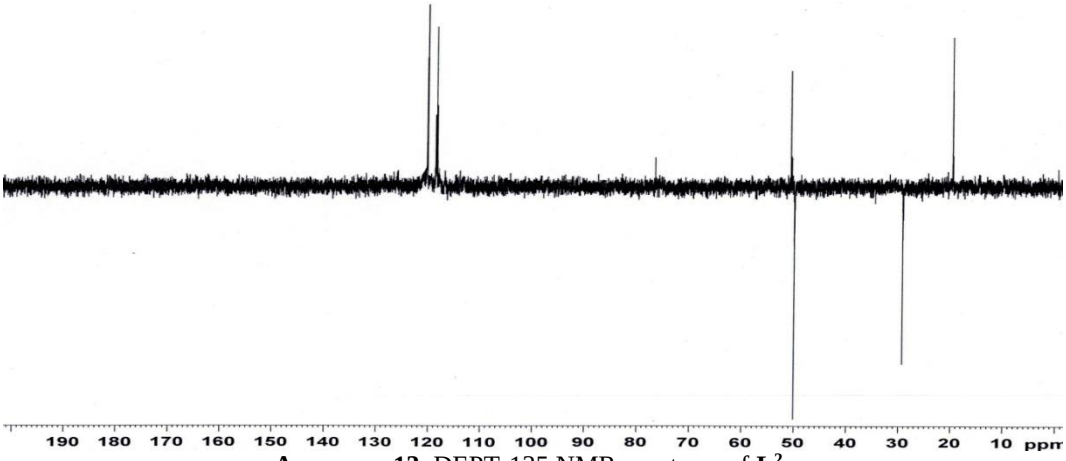

Annexure 13. DEPT-135 NMR spectrum of **L²**.

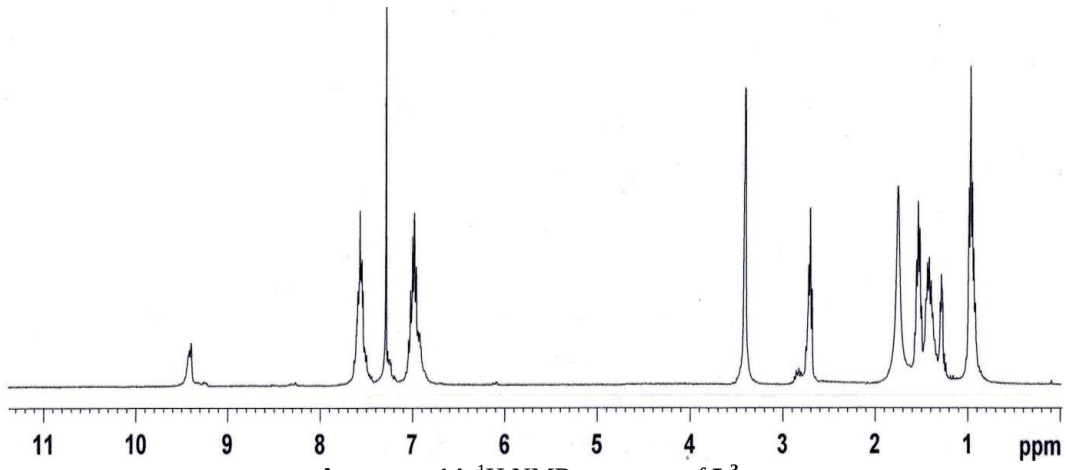

Annexure 14. ^{1}H NMR spectrum of **L³**.

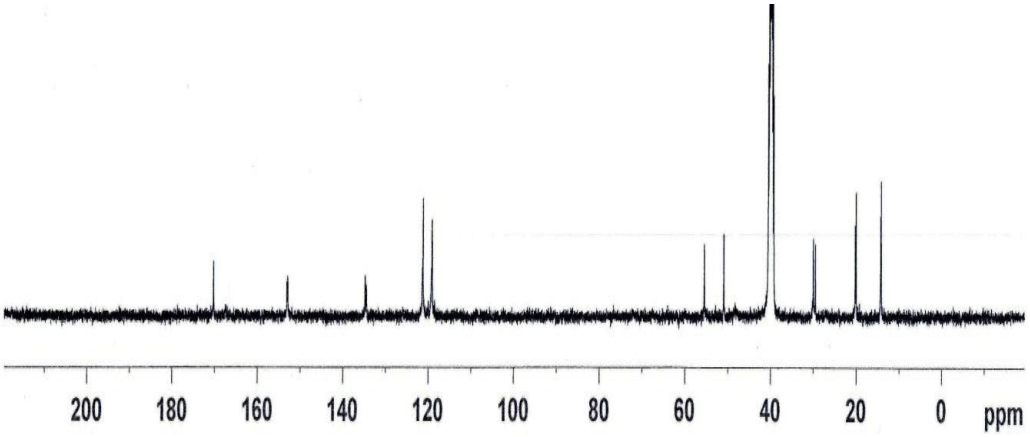

Annexure 15. ^{13}C NMR spectrum of **L^{3}**.

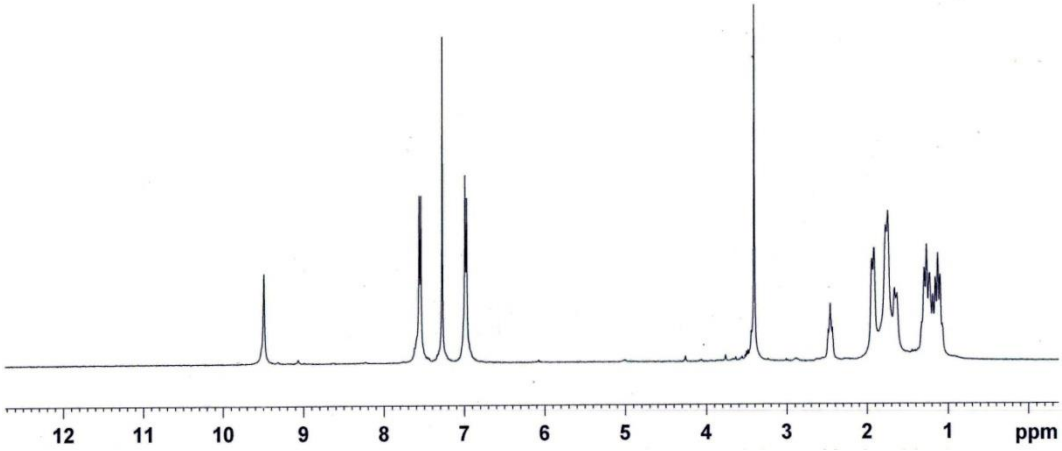

Annexure 16. ^{1}H NMR spectrum of **L^{4}**.

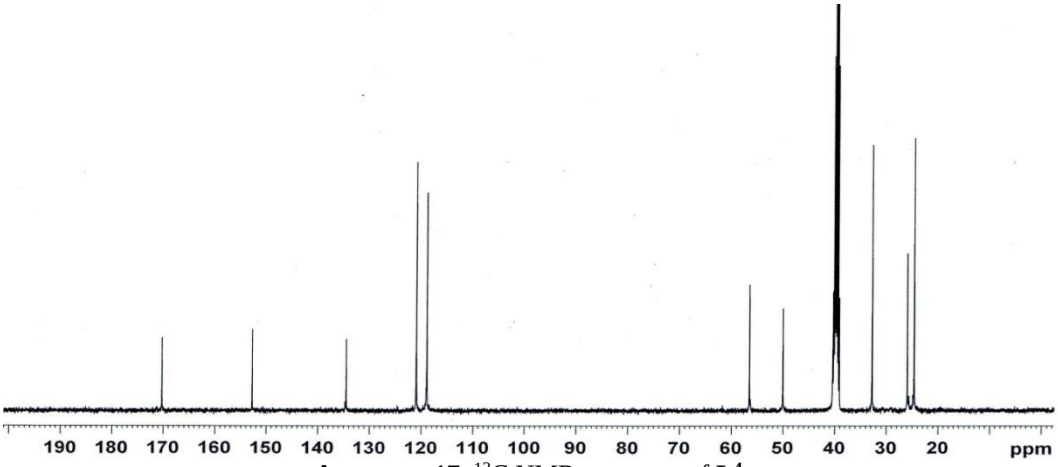

Annexure 17. ^{13}C NMR spectrum of **L^{4}**.

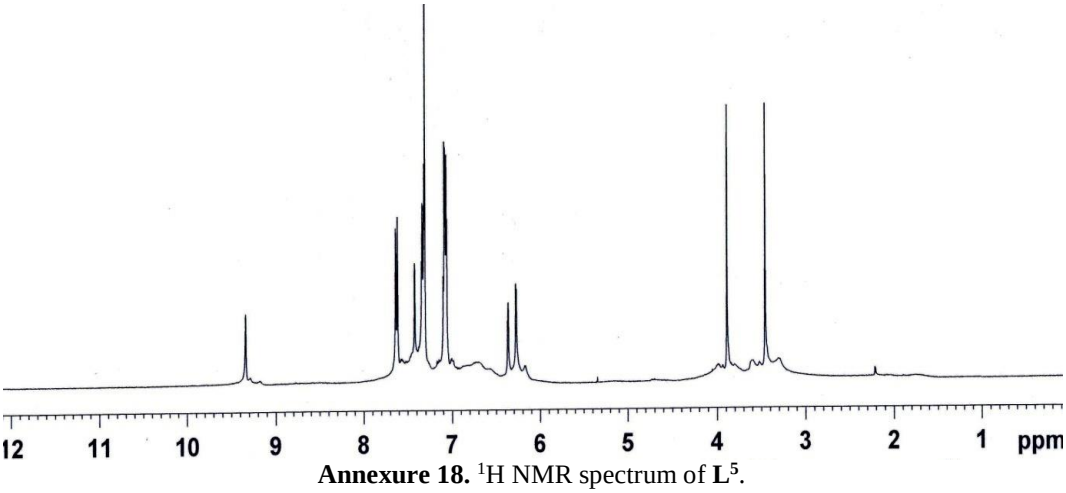

Annexure 18. ^{1}H NMR spectrum of **L^{5}**.

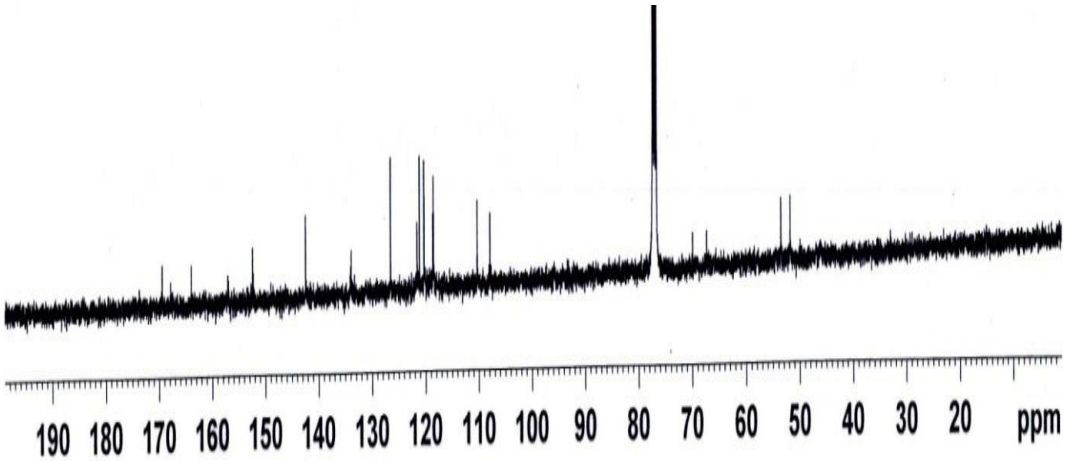

Annexure 19. ^{13}C NMR spectrum of **L^{5}**.

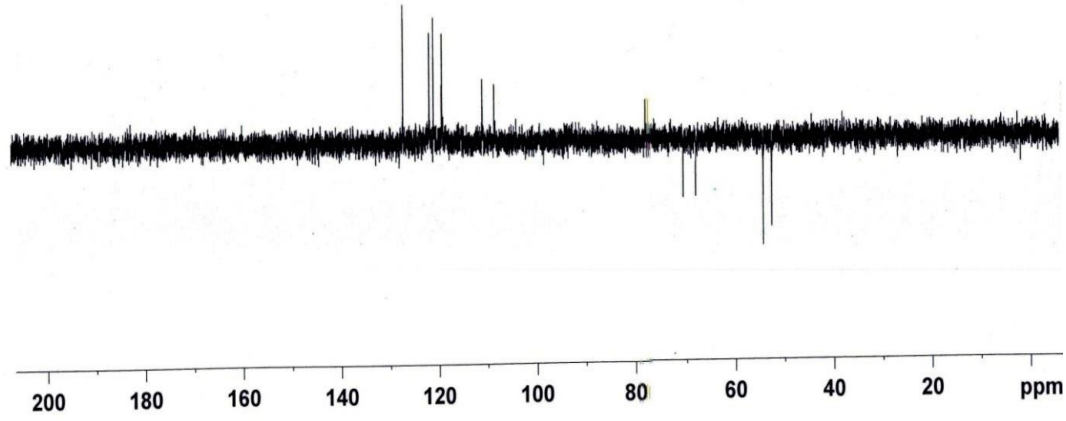

Annexure 20. DEPT-135 NMR spectrum of **L^{5}**.

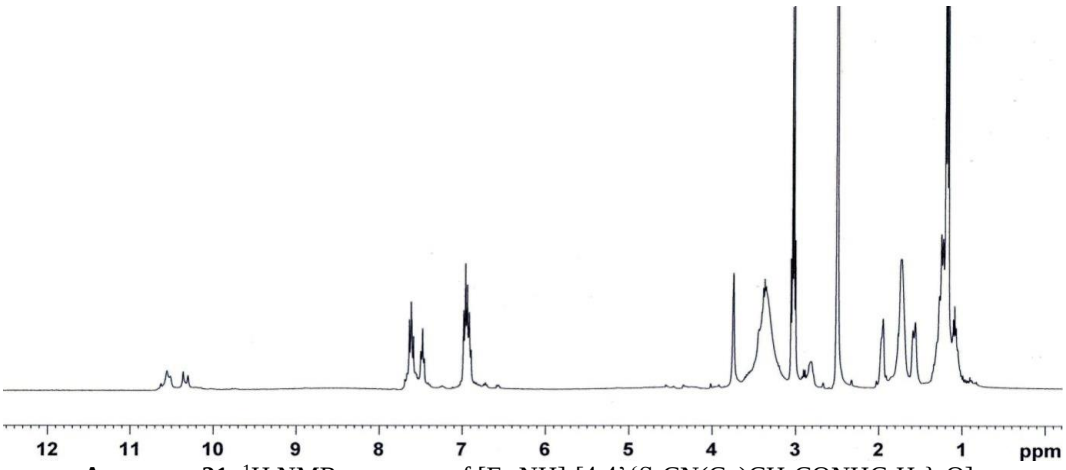

Annexure 21. ^{1}H NMR spectrum of $[Et_3NH]_2[4,4'\{S_2CN(Cy)CH_2CONHC_6H_4\}_2O]$.

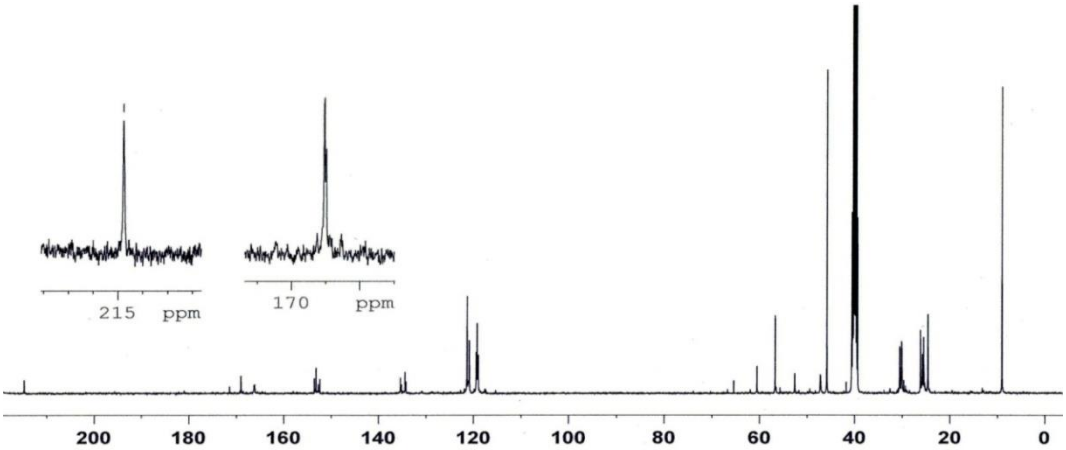

Annexure 22. ^{13}C NMR spectrum of $[Et_3NH]_2[4,4'\{S_2CN(Cy)CH_2CONHC_6H_4\}_2O]$.

$[Et_3NH]_2[4,4'\{S_2CN(Cy)CH_2CONHC_6H_4\}_2O]$: ^{1}H NMR (400 MHz, DMSO-d_6): δ (ppm) 10.6-10.3 (N*H*CO), 7.6-7.5 (m, H, Ph), 6.9 (m, H, Ph), 3.8 (s, NC*H*$_2$CO), 3.3 (m, C*H* of Cy), 3.1 (m, C*H*$_2$ of Et_3N), 2.0-1.4 (m, C*H*$_2$ of Cy), 1.2 (m, C*H*$_3$ of Et_3N). ^{13}C NMR(400 MHz, DMSO-d_6): δ (ppm) 214.79 (NCSS), 171, 169.04, 165 (CO); 153.56, 153.20, 152.72, 152.38, 135.40, 135.18, 134.18, 134.18, 121.35, 120.87, 119.42, 119.24, 119.12, 118.96 (all corresponds to the carbons of Ph), 65.38, 60.51, 56.67, 52.56 (*C*H$_2$ of NCH$_2$CO and *C*H of Cy), 45.82 (C*H*$_2$ of Et_3N), 30.47, 30.08, 26.11, 25.71, 25.45, 24.55 (*C*H$_2$ of Cy), 9.01 (C*H*$_3$ of Et_3N).

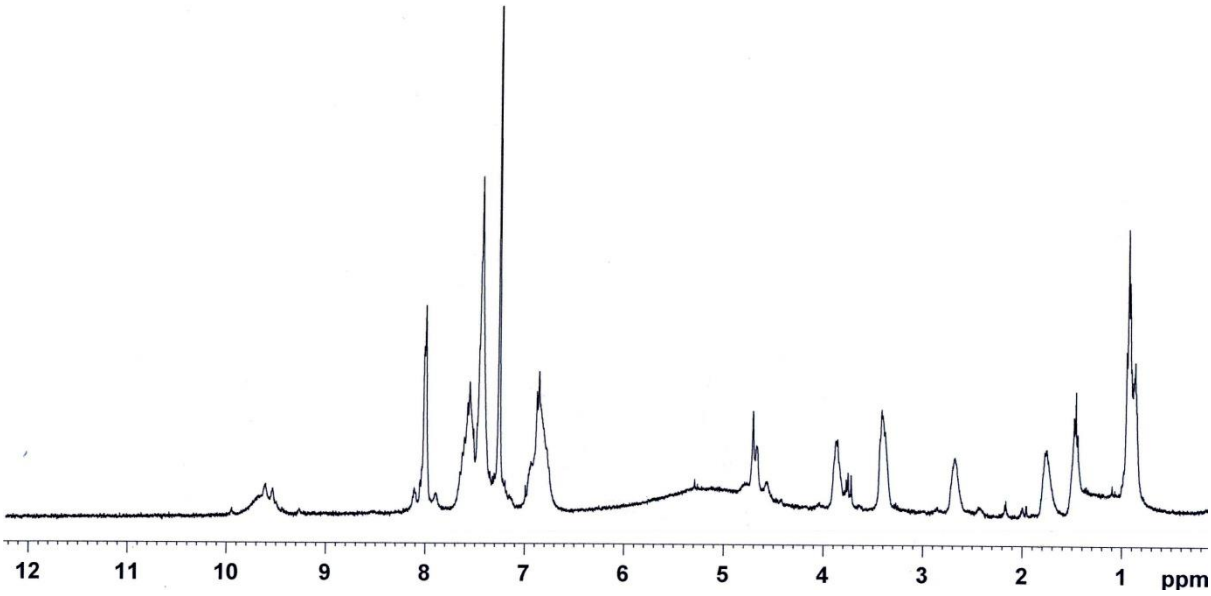

Annexure 23. ^{1}H NMR spectrum of **3**.

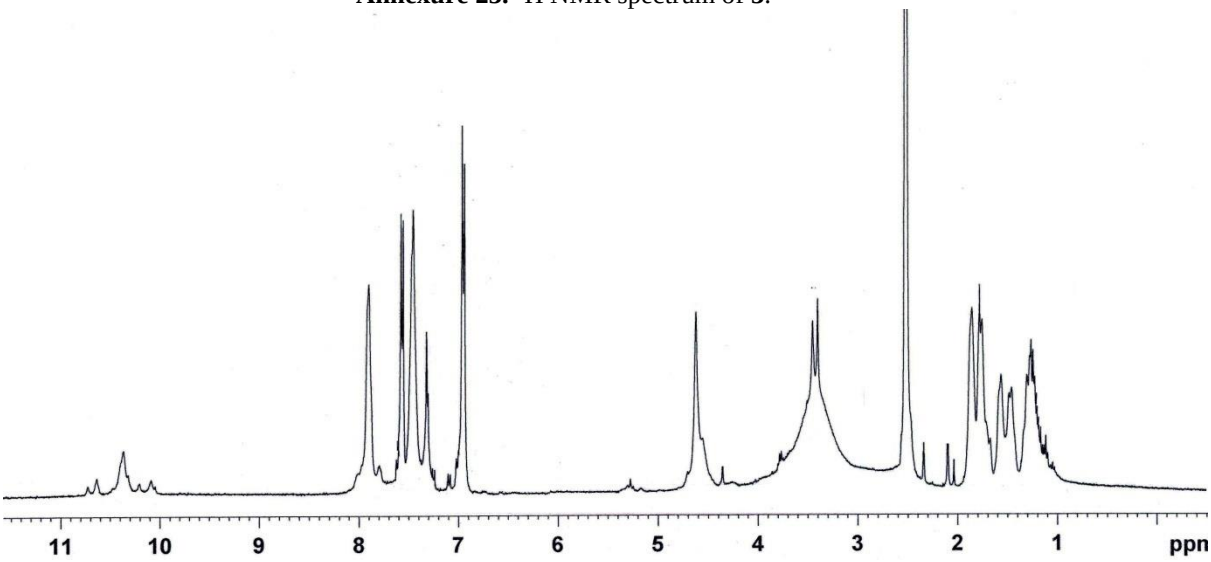

Annexure 24. ^{1}H NMR spectrum of **4**.

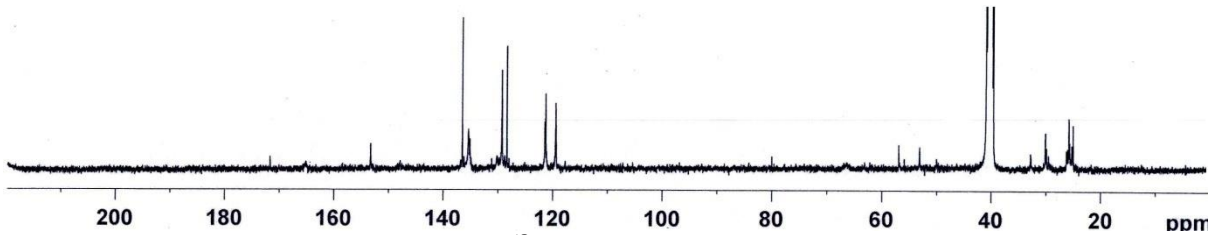

Annexure 25. ^{13}C NMR spectrum of **4**.

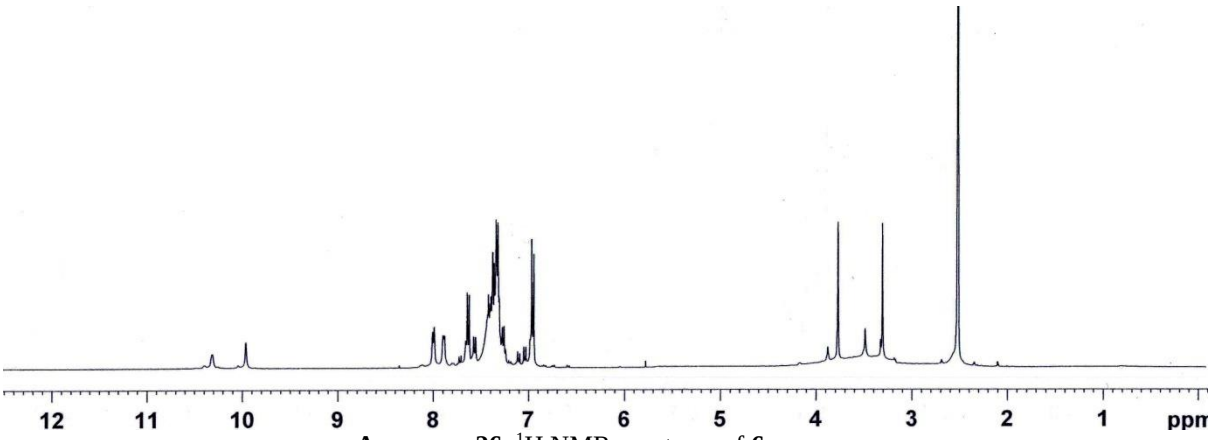

Annexure 26. ^{1}H NMR spectrum of **6**.

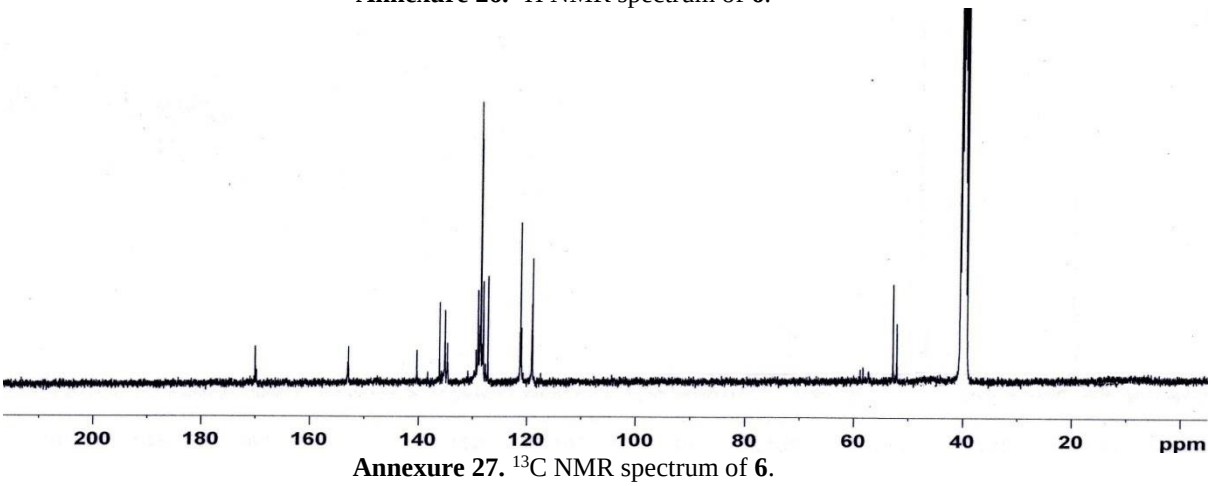

Annexure 27. ^{13}C NMR spectrum of **6**.

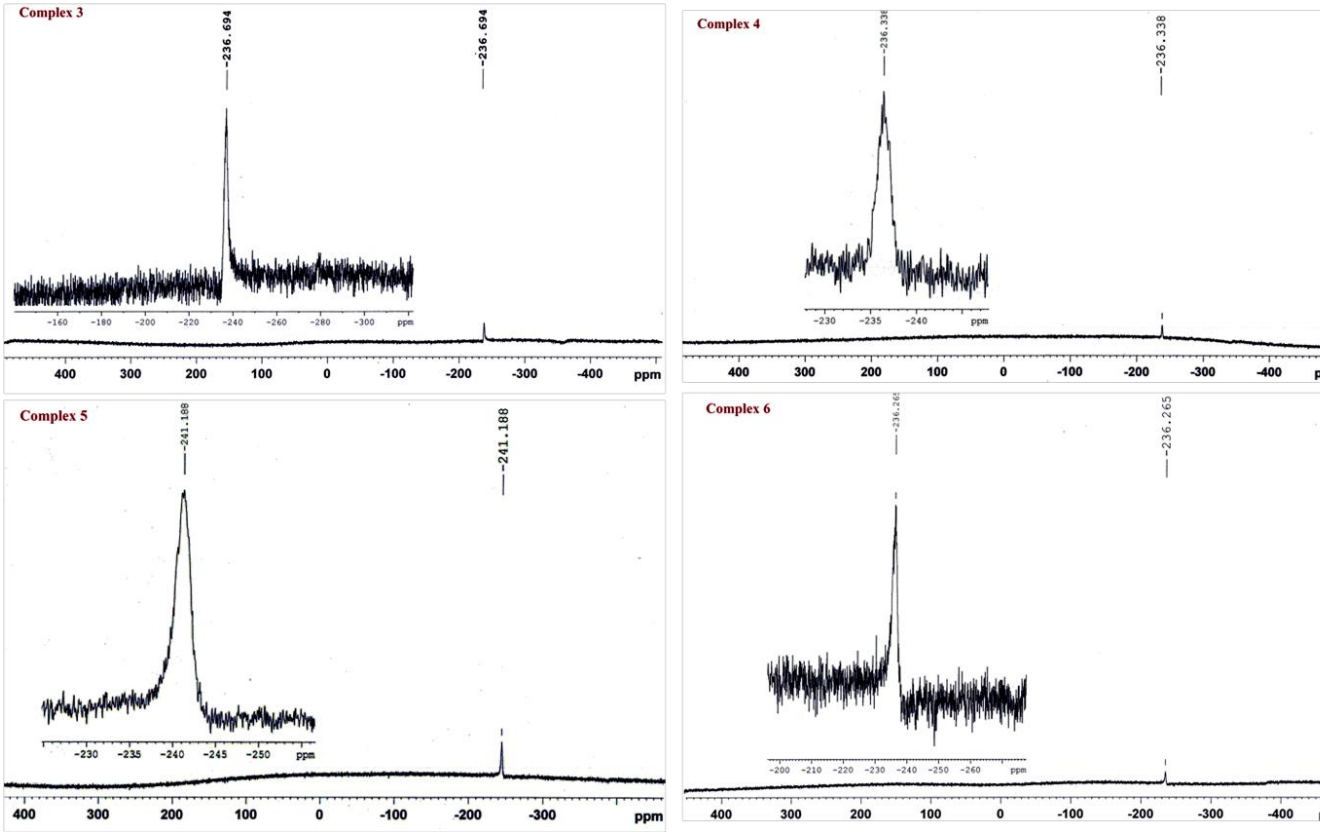

Annexure 28. ^{119}Sn NMR spectrum of **3**-**6**.

4.6.2. Computational Investigations:

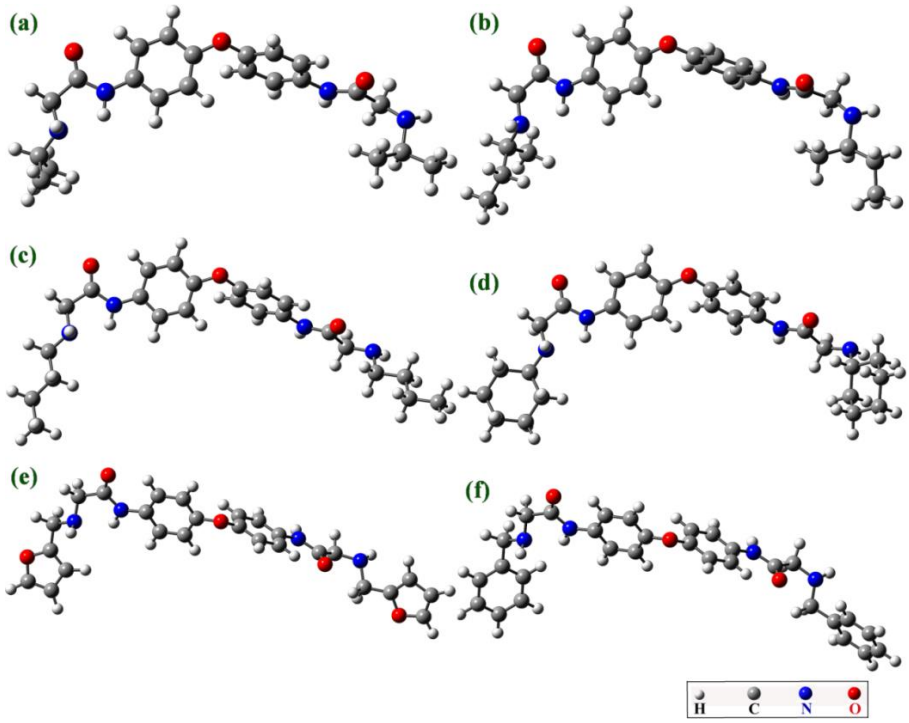

Annexure 29. An optimized geometry for the minimum energy conformation of diamine precursors **L**[1](a), **L**[2](b), **L**[3](c), **L**[4](d), **L**[5](e) and **L**[6](f) at B3LYP/6-31G (d, p) level.

The selected stereoelectronic parameters of optimized geometries for diamine precursors **L**[1]**-L**[6] are summarized in the following table A1.

Table A1. Summary of computational studies[a] performed on diamine precursors **L**[1]**-L**[6].

Entry	E_{opt} 10^6 (kcalmol^{-1})	Amine (º) C—N—C	Etherial (º) Ph—O—Ph	E_{HOMO}, E_{LUMO} (eV)	$\Delta E_{HOMO-LUMO}$ (eV)	λ_{max} calc. (expt.) nm
L$_1$	-0.8165	115.69 116.29	120.18	-5.3038 -0.2792	5.0246	247 (292)
L$_2$	-0.8658	115.82 116.53	120.24	-5.2855 -0.2634	5.0221	247 (302)
L$_3$	-0.8658	114.35 114.70	120.18	-5.3079 -0.2759	5.0319	246 (294)
L$_4$	-0.9630	116.26 116.74	120.29	-5.2779 -0.2555	5.0224	247 (297)
L$_5$	-1.0050	113.96 114.60	120.23	-5.4224 -0.3973	5.0251	247 (297)
L$_6$	-1.0078	113.97 114.80	120.26	-5.3617 -0.4367	4.9250	252 (297)

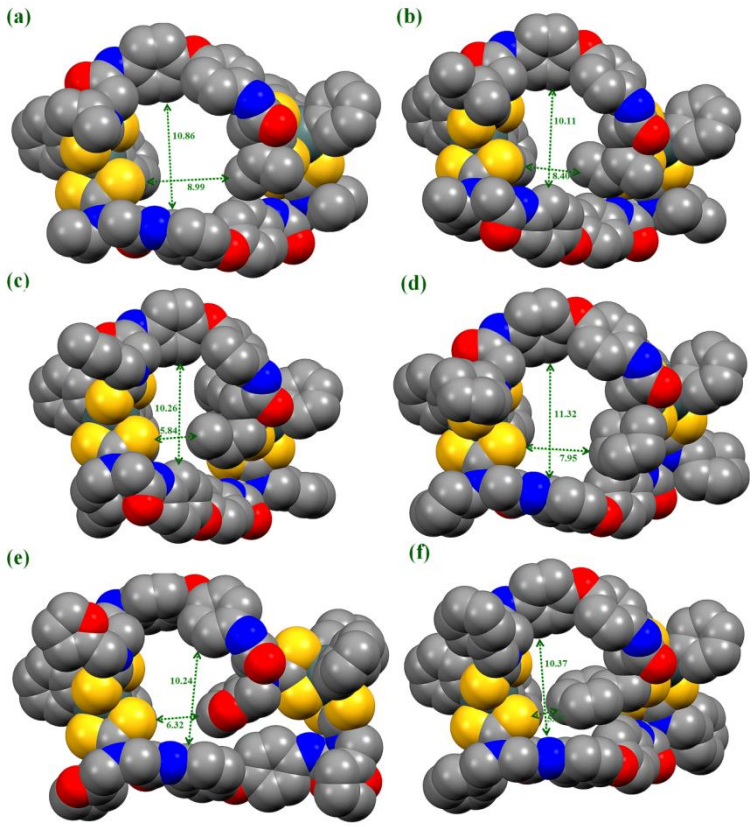

Annexure 30. An optimized geometry in spacefilled model revealing cavity generated by macrocyclic architecture of dinuclear Ph_2Sn^{IV}dithiocarbamate complexes **1**(a), **2**(b), **3**(c), **4**(d), **5**(e) and **6**(f).

Frontier molecular orbitals energies for ligand precursors:

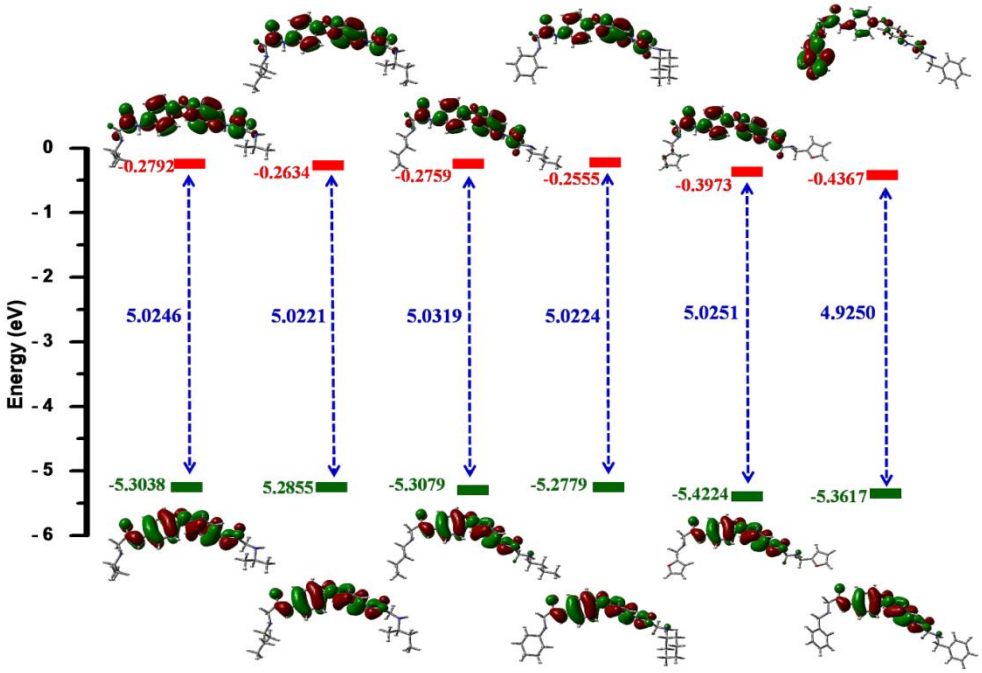

Annexure 31. Frontier molecular orbitals derived from DFT calculation at B3LYP/6-31G (d, p) level for diamine precursors $\mathbf{L^1}$-$\mathbf{L^6}$ (Isovalue= 0.02): for $\mathbf{L^1}$(a), $\mathbf{L^2}$(b), $\mathbf{L^3}$(c), $\mathbf{L^4}$(d), $\mathbf{L^5}$(e) and $\mathbf{L^6}$(f) .

The geometrical parameters for **L^1-L^6** are found to be in good agreement with those experimentally determined parameters for the similar compounds. For instance the ethereal bond angle Ph-O-Ph of ~120.2° theoretically obtained for **L^1-L^6** is comparable with the experimentally determined ethereal bond angle 4,4'-bis(benzylamino)diphenyl ether.[23] The data obtained for ligand precursors **L^1-L^6** suggest the similar type of molecular conformation with insignificant variation in the structural parameters by increasing bulkiness of the amine N-substituents. An optimized geometry for ligand precursors suggests the minimal energy '*gauche*' conformation of adjacent aromatic rings. It appears that the various amine N-substituents causes significant changes in the amine C—N—C bond angles to compensate the steric strain induced. Contrarily, the HOMO of **L^6** is localized at the phenyl rings adjacent to ethereal oxygen and LUMO is predominantly located on one of the peripheral phenyl ring whereas these orbitals are delocalized over the π-system of ethereal phenyl rings in **L^1-L^5**.

4.6.3. Cytotoxicity Study

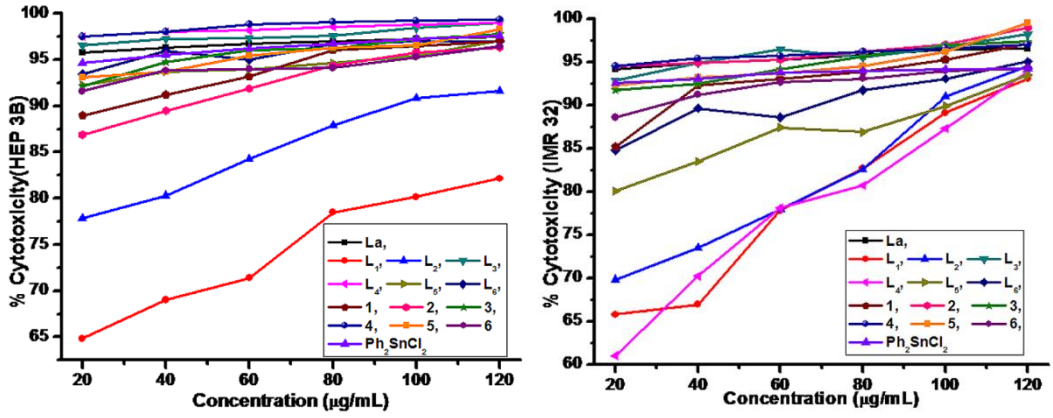

(a) **(b)**

Annexure 32. Cytotoxicity (%) for **L^a**, **L^1-L^6**, **1-6** and **Ph_2SnCl_2** against HEP 3B (a); IMR 32 (b) cell lines.

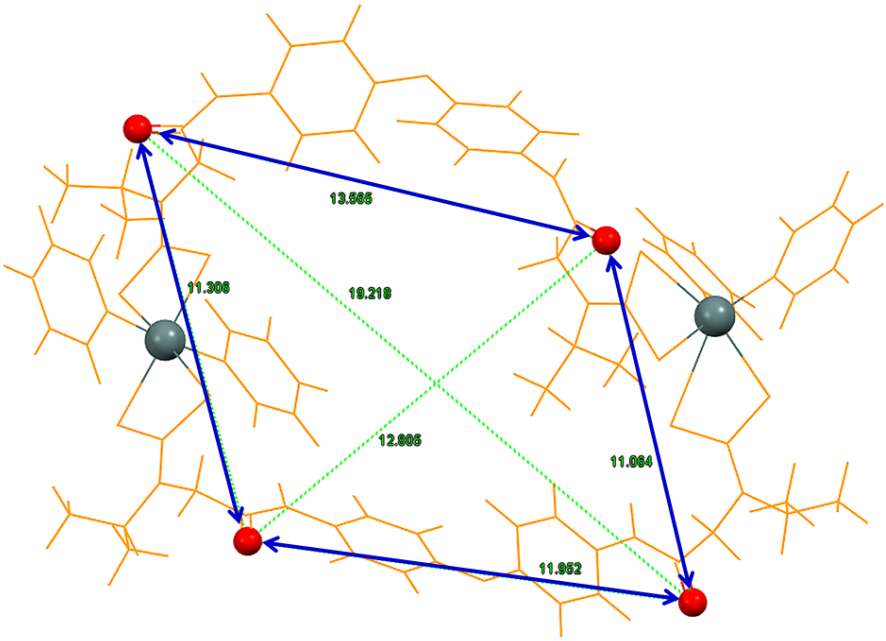

Annexure 33. View of an optimized geometry of **1** revealing position of amide moiety.

Table A2. Parameters obtained from the computational investigations and cytotoxic activity for model compounds.

Entry	E_{LUMO} (eV)	ΔE_{H-L} (eV)	Charges on chelated atoms N/S and/or Sn centre	Bite angle of Ph rings
L_1	-0.2792	5.0246	N -(0.461- 0.540)	…
L_2	-0.2634	5.0221	N -(0.472- 0.550)	…
L_3	-0.2759	5.0319	N -(0.488- 0.553)	…
L_4	-0.2555	5.0224	N -(0.486- 0.548)	…
L_5	-0.3973	5.0251	N -(0.496- 0.555)	…
L_6	-0.4367	4.9250	N -(0.480- 0.544)	…
1	- 1.3448	4.0263	N -(0.282- 0.301) S -(0.122-0.280) Sn (1.051-1.060)	113.89, 101.98
2	- 1.4934	3.8140	N -(0.284- 0.305) S -(0.118-0.285) Sn (1.047-1.060)	114.84, 102.14
3	- 1.6213	3.6545	N -(0.273- 0.295) S -(0.111-0.285) Sn (1.048-1.060)	115.53, 103.31
4	- 1.2912	4.0230	N -(0.278- 0.300) S -(0.126-0.274) Sn (1.056-1.059)	113.73, 102.01
5	- 1.4346	3.8546	N -(0.271- 0.290) S -(0.128-0.265) Sn (1.054-1.057)	114.77, 101.88
6	- 1.4798	3.8663	N -(0.272- 0.289) S -(0.118-0.277) Sn (1.049-1.059)	116.23, 103.09

4.6.4. Thermogravimetric Analysis

Table A3. Thermogravimetric analysis of diamine ligand precursors **L^1-L^6** and binuclear diphenyltin^{IV}dithiocarbamate complexes **1–6**.

Entry	DTG (°C) (μg/min)	% Mass loss (temp range °C)	Inference
L^1	128.2 (79.6), 186.3 (216.6), 225.8 (78.4), 351.8 (29.3), 491.0 (15.6).	28.80% (120-550)	Multistage mass loss due to removal of molecular fragments. Maximum rate of decomposition observed at 186.3 °C on DTG curve. Decomposition continues after 550 °C.
L^2	79.2 (47.2), 170.2 (133.4), 183.3 (162.0), 236.0 (58.6), 184.7 (107.8).	2.07% (60-150), 27.93 (150-550), 30.0% (50-550)	1st stage: insignificant mass loss due to removal of solvent impurities. 2nd stage: mass loss due to removal of molecular fragments. Maximum rate of decomposition observed at 183.3 °C on DTG curve. Decomposition continues after 550 °C.
L^3	303.3 (197.2), 349.5 (247.6)	0.8% (100-200), 70.4% (200-550), 71.2% (50-550)	1st stage: insignificant mass loss due to removal of solvent impurities. 2nd stage: mass loss due to removal of molecular fragments. Maximum rate of decomposition observed at 349.5 °C on DTG curve. Complete decomposition of molecular fragments leaving char.
L^4	127.1 (15), 362.1 (477)	91.3% (250-550)	1st stage: mass loss due to removal of molecular fragments. Maximum rate of decomposition observed at 362.1 °C on DTG curve. Complete decomposition of molecular fragments leaving char. *An endothermic peak at 137.7 °C appeared on DTA curve without mass loss suggesting phase changes occurring due to its melting.*
L^5	168.7 (3.3), 272.4 (68.4), 292.3 (72.6), 401.3 (26.3)	0.13% (80-200), 40.91% (200-550), 41.04% (50-550)	1st stage: insignificant mass loss due to removal of solvent impurities. 2nd stage: mass loss due to removal of molecular fragments. Maximum rate of decomposition observed at 292.3 °C on DTG curve. Decomposition continues after 550 °C.
L^6	342.9 (0.250)	83.9% (200-550)	1st stage: mass loss due to removal of molecular fragments. Maximum rate of decomposition observed at 342.9 °C on DTG curve. Complete decomposition of molecular fragments leaving char. *An endothermic peak at 128.4 °C appeared on DTA curve without mass loss suggesting phase changes occurring due to its melting.*
1	152.3 (27.1), 173.2 (27.5), 271.5 (198.9)	1.2% (80-120), 33.4% (120-550), 34.6% (50-550)	1st stage: insignificant mass loss due to removal of solvent impurities. 2nd stage: mass loss due to removal of molecular fragments. Maximum rate of decomposition observed at 271.5 °C on DTG curve. Decomposition continues after 550 °C.
2	154.5(26.9), 173.6 (20.4),	1.1% (80-120), 35.4% (120-550),	1st stage: insignificant mass loss due to removal of solvent impurities.

	276.9 (227.2)	36.5% (50-550)	2nd stage: mass loss due to removal of molecular fragments. Maximum rate of decomposition observed at 276.9 °C on DTG curve. Decomposition continues after 550 °C.
3	105.5 (379), 135.7 (0.112), 230.4 (744)	86.4% (100-400),	Multistage mass loss due to removal of molecular fragments. Maximum rate of decomposition observed at 230.4 °C on DTG curve. Complete decomposition probably due to formation of volatile products.
4	114.7 (65.9), 213.5 (110.3), 283.6 (47.5), 358.8 (39.7)	63.5% (100-550),	Multistage mass loss due to removal of molecular fragments. Maximum rate of decomposition observed at 213.5 °C on DTG curve. Decomposition continues after 550 °C.
5	101.1 (231.3), 206.0 (226.6), 226.9 (0.206)	13.0% (100-150), 37.7% (150-250), 50.7% (50-550)	Multistage mass loss due to removal of molecular fragments. Maximum rate of decomposition observed at 101.1 °C on DTG curve. Decomposition continues after 550 °C.
6	123.3 (10.2), 156.0 (8.8), 266.6(75.4), 370.8 (23.4)	57.4% (100-550) 57.4% (50-550	Multistage mass loss due to removal of molecular fragments. Maximum rate of decomposition observed at 226.6 °C on DTG curve. Decomposition continues after 550 °C.

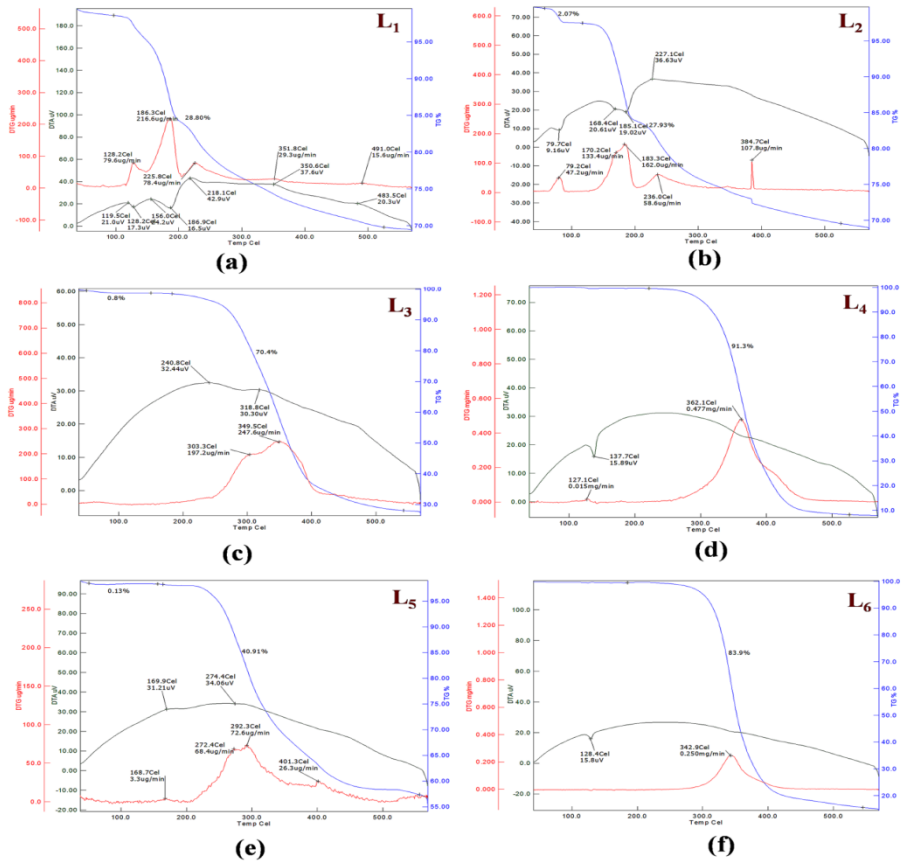

Annexure 34. Thermogram of diamine precursors **L**[1] (a), **L**[2] (b), **L**[3] (c), **L**[4] (d), **L**[5] (e) and **L**[6] (f).

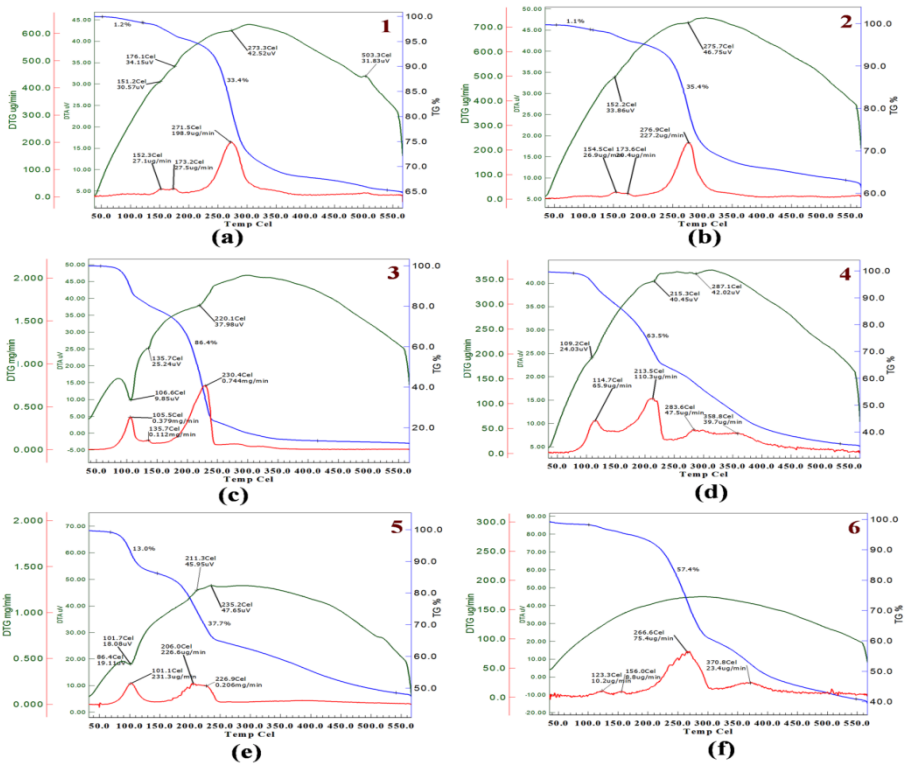

Annexure 35. Thermogram of binuclear diphenyltin^{IV}dithiocarbamate complexes **1–6**: **1** (a), **2** (b), **3** (c), **4** (d), **5** (e) and **6** (f).